Influence of modern environmental gradients on foraminiferal faunas in the inner Kongsfjorden (Svalbard)

Eleonora Fossile, Maria Pia Nardelli, Hélène Howa, Agnès Baltzer, Yohann Poprawski, Ilaria Baneschi, Marco Doveri, Meryem Mojtahid

Influence of modern environmental gradients on foraminiferal faunas in the inner Kongsfjorden (Svalbard)

Eleonora Fossile[1*], Maria Pia Nardelli[1], Hélène Howa[1], Agnes Baltzer[2], Yohann Poprawski[1], Ilaria Baneschi[3], Marco Doveri[3], Meryem Mojtahid[1]

[1] LPG-BIAF, UMR CNRS 6112, Univ Angers, 2 Bd Lavoisier, 49045 Angers Cedex 01, France

[2] LETG, UMR CNRS 6554, University of Nantes, Campus du Tertre, 44312 Nantes Cedex 3, France

[3] Istituto di Geoscienze e Georisorse IGG-CNR, Via Moruzzi 1, 56100 Pisa, Italy

*Correspondence to: Eleonora Fossile (eleonora.fossile@gmail.com)

Keywords: benthic foraminifera, bioindicators, tidewater glacier, Arctic, fjord hydrology

Abstract

The Kongsfjorden, an Arctic fjord located in the north-western Svalbard archipelago, is influenced by the Atlantic Water (AW) inflow from the shelf as well as by tidewater glacier dynamics at the fjord head. This generates strong environmental gradients across the fjord creating high physical and geochemical stress for the benthic faunas. This research focuses on the study of benthic foraminiferal faunas under present-day environmental conditions (during summer 2018) in the inner Kongsfjorden, with the aim at understanding the main environmental factors governing their distribution and species composition. To that aim, surface sediments from 9 stations were sampled during August 2018 following a transect along the main axis of the fjord, from near the front (ca. 2 km) of the tidewater glaciers Kronebreen and to about 12 km seaward. The results show that the distribution of foraminiferal assemblages was influenced by the dual effect of the proximity of the glacier front and the AW inflow and the associated hydrological, sedimentary, and food export processes. These resulted in the succession of three ecological groups along the inner fjord axis, responding to physical disturbances linked to the proximity of the Kronebreen terminus (i.e., high water turbidity, freshwater, and sediment inputs from subglacial discharges). Close to the glacier front, few stress-tolerant and glacier proximal species were present (i.e., *Capsammina bowmanni* and *Cassidulina reniforme*). At about 6-8 km from the glacier front, reduced turbidity, and an increase in organic matter fluxes (likely related to an increase in primary production), resulted in a higher foraminiferal diversity, and a high abundance of the phytodetritus-indicator *Nonionellina labradorica*. Relatively high taxonomic diversity persists until 12 km from the glacier front due to higher organic inputs and reduced stressful conditions (i.e., decreasing freshwater and sediment inputs). The outer assemblage was dominated by the AW indicator *Adercotryma glomeratum*, in coherence with the presence of warm and salty AW far inside the Kongsfjorden during the sampling period. Physical stress related to the glacier dynamics appears to favour the establishment of an opportunistic pioneer assemblage close to the terminus, whereas reduced disturbance away from the glacier induces the establishment of

diverse foraminiferal assemblages. Based on the strong response of benthic foraminifera on a kilometric scale, they may be effective bioindicators for annual monitoring the long-term retreat of tidewater glaciers as a result of climate change in Kongsfjorden.

1. Introduction

The ongoing climate change is threatening the Arctic region at faster rate compared to lower latitudes (IPCC, 2019). In the last decades, the Arctic warming doubled the global mean, a phenomenon called Arctic amplification (AA - Dai et al., 2019; Holland and Bitz, 2003). Although the exact causes of the AA are still debated, the scientific community agrees that it is mainly the result of both local feedbacks (e.g. ice-albedo - Screen and Simmonds, 2010; Stuecker et al., 2018) and climatic/oceanographic forcing (e.g. changes in poleward heat transport - Graversen et al., 2008; Screen et al., 2012). The rapid sea ice cover shrinking and glacier mass loss is a striking evidence of climate change in the Arctic (IPCC, 2019). The climate change-induced increase in ocean temperature and reduction in water stratification are among the causes of the sea ice decline in the Arctic Ocean (e.g. Lind et al., 2018; Polyakov et al., 2017; Yu et al., 2021). For land-terminating glaciers, the major mechanism for melting is through surface meltwaters migrating to the ice-bedrock interface (e.g. Tedstone et al., 2015; Zwally et al., 2002), whereas ocean-terminating glaciers mainly lose mass through calving at the glacial front by warming seawater temperatures (e.g., Luckman et al., 2015). Whether through rising sea temperatures or changes in freshwater and sediment inputs induced by glacier melting, these climate change-induced phenomena are having, and will continue to have, several implications for Arctic marine ecosystems, with repercussions on the benthic and pelagic realms (Meredith et al., 2019).

The Svalbard archipelago (74-81°N and 10-35°E) is largely influenced by the warm and saline Atlantic Water (AW). The AW, carried by the North Atlantic Current (NAC) and further north by the West Spitsbergen Current (WSC), flows west of the archipelago and enters the Arctic Ocean as the major source of heat, carbon, and plankton (e.g., Vernet et al., 2019) (Fig.

1). Western Svalbard fjords, located close to the WSC path, experience an increasing influence of warm and saline AW, more than any other Arctic fjords (Cottier et al., 2007; Saloranta and Svendsen, 2001). Furthermore, the mean temperature of the WSC core (20-200 m depth) has increased by 0.7°C in the last 20 years (Norwegian Polar Institute, 2021). Beside the climatic modifications, the hydrological conditions of the fjord are also subjected to extreme seasonal variations. During summer, warm AW incursions and freshwater inputs from glaciers, determine the presence of strong temperature and salinity gradients across these systems (e.g. Cottier et al., 2010; Hop et al., 2002; Hop and Wiencke, 2019; Svendsen et al., 2002). The fjords, through circulation dynamics and mixing between fjord and shelf waters (i.e. an inshore dominated by glaciers with seasonal meltwater inputs and an offshore influenced by warm oceanic water intrusions), represent a link between the ocean and the land (Cottier et al., 2010). Therefore, these systems are submitted to combined variations of these two end-members and are thus sensitive to seasonal climatic fluctuations and to oceanographic changes (Cottier et al., 2005).

The Kongsfjorden, a glacially, over-deepened valley located in the north-western coast of Spitsbergen, is influenced by the AW circulation as well as by tidewater glacier dynamics and the associated water masses at the fjord head (Hop et al., 2002; Sundfjord et al., 2017; Svendsen et al., 2002). Nowadays, this fjord is experiencing important changes. Before 2006, extensive sea ice was formed each winter in the inner fjord, but since then, the increased inflow of AW and the resulting overall increasing trend in seawater temperatures (e.g., Cottier et al., 2007; David T and K.P., 2017; Payne and Roesler, 2019; Tverberg et al., 2019) shifted the fjord system into a warmer state (Cottier et al., 2010, 2007). This resulted in a reduced sea ice cover (i.e., up to 50% decrease; Pavlova et al., 2019) and thickness (i.e., from 0.6 m to 0.2 m decrease; Pavlova et al., 2019).

In summer, it has been reported that AW intrusion in the Kongsfjorden occurred during prolonged periods of time, and that AW has reached the inner part of the fjord only in the last decade (Holmes et al., 2019). This recent hydrological change strongly enhanced submarine melt and calving (i.e., frontal ablation) of tidewater glaciers (Holmes et al., 2019; Luckman et

al., 2015), and consequently increased meltwater discharges and associated sediment load at the fjord head. As a result, the higher water turbidity in the vicinity of the marine termini of Kronebreen and Kongsvegen glaciers reduces local euphotic depth, disrupting phytoplankton distribution and biomass at the Kongsfjorden head (Payne and Roesler, 2019). Furthermore, glacial meltwater runoff has a direct implication in building up steep temperature and salinity vertical gradients that lead to stable water stratification in the fjord. As a consequence primary production is even more affected with repercussions on the entire trophic chain (Pasculli et al., 2020). Knowing that marine-terminating glaciers generally sustain high productivity in arctic fjords (Meire et al., 2017), the recent seasonal processes developing in the Kongsfjorden may cause persistent physical and geochemical stresses with impact on the fjord ecosystem, particularly on the benthic faunas.

The impact of increasing glacial melting on the Arctic marine ecosystems remains poorly studied (Meire et al., 2017), and a better understanding of the resilience capability of fjord ecosystems under present-day evolving conditions is needed (Hop et al., 2019). To that aim, benthic foraminifera are powerful and promising tools. Thanks to their short life cycle and specific ecological requirements, they respond quickly to environmental disturbance (e.g., Jorissen et al., 1995; Hald and Korsun, 1997; Alve et al., 2016; Jernas et al., 2018). Moreover, their fossilisation potential allows historical and paleoenvironmental reconstructions (e.g., Skirbekk et al., 2010; Jernas et al., 2013; Pawłowska et al., 2017) providing critical information on the evolution of a similar habitat in the recent past (e.g., tens to hundreds of years).

The present study focuses on the ecology of benthic foraminiferal faunas under current environmental conditions in the inner Kongsfjorden, with the aim of understanding the main drivers of benthic communities in fjords influenced by glacier dynamics and in a warm state. Foraminiferal distribution was analysed in response to the steep environmental gradients created by the meltwater runoff from tidewater glaciers at the fjord head and the AW inflow at the fjord mouth in summer.

2. Study area

2.1. Geographical and geological setting

The Kongsfjorden is a glaciomarine fjord (20 km long and 4-10 km wide) located on the north western coast of Spitsbergen (79°N, 12° E) in the Svalbard archipelago. This fjord, elongated in the SE-NW direction, is located on a tectonic boundary between the Tertiary Fold and Thrust Belt to the south-west thrusting on the Northwestern Basement Province to the north-east (Bergh et al., 2000). The Kongsfjorden has likely developed in a morphological depression linked to fractures of the bedrock, parallel to the thrust front (Husum et al., 2019; Svendsen et al., 2002).

Bedrocks of different composition are present in the fjord basement (Svendsen et al. 2002). Located on the Northwestern Basement Province, the northern bank of the fjord consists of medium-grade metamorphic (Middle Proterozoic age) marbles, mica-schists, and quartzites. The eastern part of the fjord and the islands at the fjord head (e.g., BlomstandhalvØya; Fig.1) are composed of slices of unmetamorphosed rocks (red conglomerates and sandstones) of Devonian age and marbles. Above the basal Tertiary thrust, the southern Kongsfjorden bedrock consists of sedimentary rocks of Late Palaeozoic and Tertiary Age, with some Proterozoic low- and medium-grade metamorphic rocks (mica-schists, marbles, phyllites, quartzites) (Svendsen et al., 2002).

The main source of sediment in Kongsfjorden is through subglacial discharge from tidewater glaciers (Svendsen et al., 2002; Trusel et al., 2010; D'Angelo et al., 2018). In addition, the glacial rivers of the Lovenbreen continental glaciers can provide a further supply of sediment (Bourriquen et al., 2016; 2018). Particles flux into the Kongsfjorden mainly consist of siliciclastic and detrital carbonate grains (D'Angelo et al., 2018). The bedrock geology of glacier catchments also influences the nutrient dynamics in the fjord. The sedimentary supply derived from the erosion of the surrounding bedrocks, that nourishes the Kongsfjorden waters through meltwater discharge, makes this environment rich in silicon (e.g., silica-rich bedrock

146 determines high silicic acid content in glacier meltwaters; Halbach et al., 2019) and iron
147 (Laufer-Meiser et al., 2021). Limitation of sea life will come from a deficit of fresh organic matter
148 with low C:N ratio (Laufer-Meiser et al, 2021). At the fjord head, high accumulation rates of
149 detrital material (i.e., 6-8 cm yr^{-1}; Zaborska et al., 2006; Trusel et al., 2010) and low primary
150 productivity lead to bottom sediments with low total organic carbon (TOC) content, as a result
151 of the dilution effect of lithogenic material. Laufer-Meiser et al. (2021) found organic carbon
152 with a very high C:N ratio (i.e., ratio of up to 70) in sediment close to the glacial source,
153 originating from the terrestrial input of refractory petrogenic organic carbon (more resistant to
154 microbial degradation compared to fresh marine organic carbon, Arndt et al., 2013)

155 **2.2. Oceanographic and hydrological setting**

156 The Svalbard archipelago (74-81°N and 10-35°E) is the eastern margin of the Fram Strait that
157 connects the Atlantic and Arctic Oceans. Active exchanges between northern-sourced and
158 southern-sourced water masses, that are essential for modulating the climate at various time-
159 scales occur through this gateway (Dickson et al. 2008). The Fram Strait channels the inflow
160 of the dominant heat source for the Arctic Ocean, the Atlantic Water (AW), via the West
161 Spitsbergen Current (WSC), a branch of the North Atlantic Current (Schauer et al., 2004). On
162 the western margin of Svalbard, the WSC flows northwards along the continental slope
163 whereas the Spitsbergen Polar Current (SPC), an extension of the East Spitsbergen Current
164 (ESC), transport Arctic Water (ArW) parallel on the continental shelf of Spitzbergen (Tverberg
165 et al., 2019) (Fig. 1). Cold and fresh ArW carried by SPC is separated from the warm and
166 saline AW by the Arctic front (Fig. 1).

167 The Kongsfjorden, due to its geographical location on the western margin of Svalbard, and
168 its open fjord configuration, i.e. without a well-defined sill (Howe et al. 2003), is strongly
169 influenced by oceanic intrusion derived from the Fram Strait circulation and depending on the
170 Arctic front dynamics (Svendsen et al., 2002). Water mass intrusions across this front are
171 allowed by barotropic instabilities (Saloranta and Svendsen, 2001). Frontal instabilities, due to

strong northerly winds, promote the AW upwelling from the WSC core and thus, the AW advection across the shelf into the Kongsfjorden (Cottier et al., 2005, 2007; Svendsen et al., 2002). However, the AW intrusions occur especially in summer when there is a geostrophic balance between shelf and fjord waters (Svendsen et al., 2002; Cottier et al., 2005). These cross-shelf mechanisms determine a seasonal shift between the prevailing cold and fresh ArW during winter, and the warm and saline AW during summer on the shelf and into the fjord (Svendsen et al., 2002; Cottier et al., 2005).

The spreading of AW intrusion into the fjord changes yearly, determining the distinction between “cold” and “warm” years (Cottier et al., 2005; Hop et al., 2002; Svendsen et al., 2002). Cottier et al. (2005) hypothesised that this interannual variability depends on both internal and external factors. The internal parameter would be the formation of sea ice during the preceding winter, whereas the external factor is most likely the shelf wind field creating instabilities at the shelf front during summer.

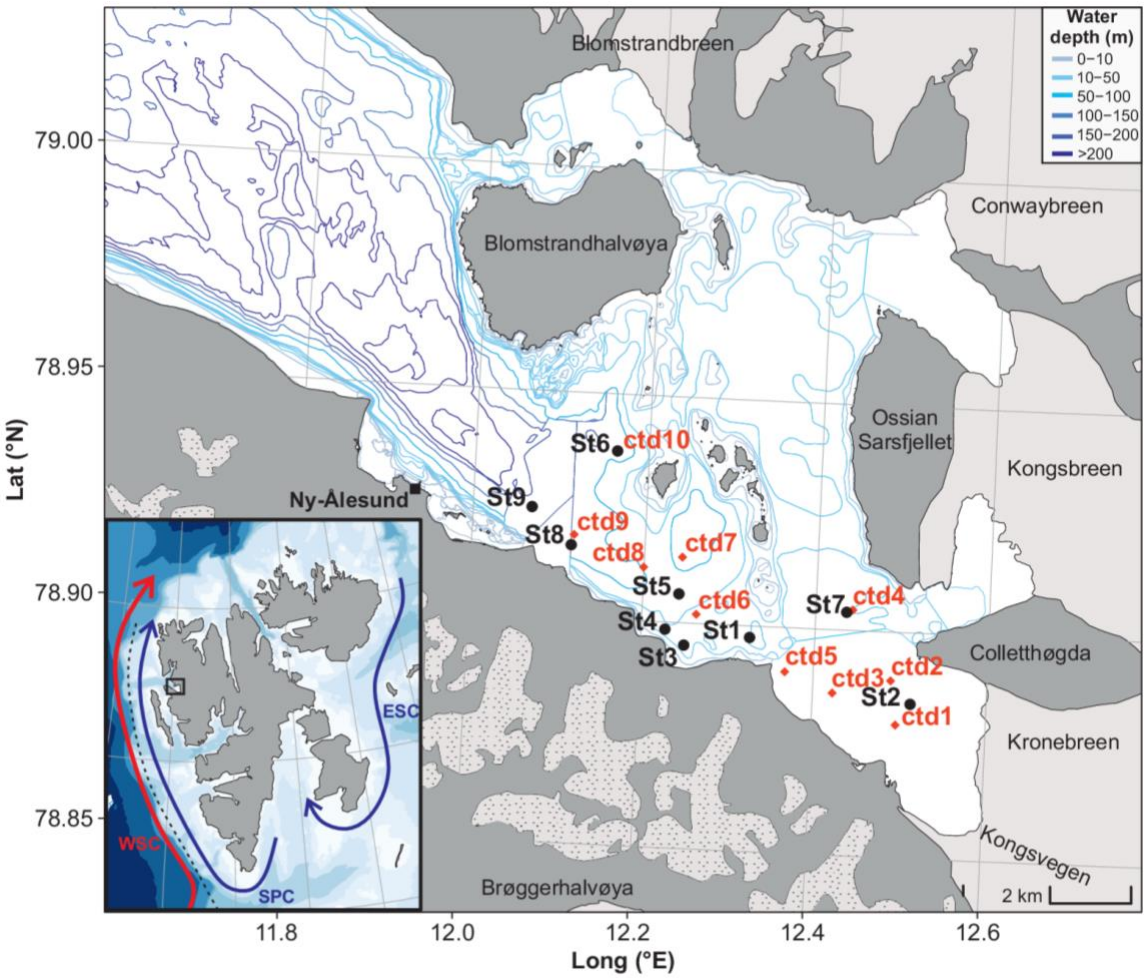

Figure 1. Map of the Kongsfjorden showing, on the eastern and northern bank, the five tidewater glaciers flowing in the fjord (light grey) and on the southern bank the continental (land terminating) glaciers (dotted light grey). The nine stations sampled with the interface corer (black dots), the ten locations of CTD cats (red squares) performed during August 2018. On the bottom left of the panel, a map of Svalbard archipelago showing the main current streams: Arctic waters (blue lines) carried by the East Spitsbergen Current (ESC) and Spitsbergen Polar Current (SPC), and Atlantic waters transported by the West Spitsbergen Current (WSC). The dashed black line represents the Arctic front west of Spitsbergen. The map was performed with the R package PlotSvalbard (Vihtakari, 2020).

The Kongsfjorden is surrounded by four continental (land-terminating) glaciers (Estre Lovenbreen, Midtre Lovenbreen, Westre Lovenbreen, and Pedersenbreen) and five tidewater (marine-terminating) glaciers (Blomstrandbreen, Conwaybreen, Kongsbreen, Kronebreen and Kongsvegen; Fig. 1). During summer, those tidewater glaciers highly contribute to the fjord dynamics with important freshwater and sediment inputs. Kronebreen, a fast-flowing tidewater

glacier, has one of the highest flux rates in Svalbard (winter speed of 1.5-2 m d^{-1}, with 3-4 m d^{-1} peaks in summer; Luckman et al., 2015).

Due to the dual influence of AW inflow and freshwater inputs from glacier meltwaters, the Kongsfjorden is characterised by different seasonal water masses. Cottier et al. (2005) revised the classification of these water masses based on Svendsen et al. (2002). Most of the AW entering the fjord mixes with ArW on the shelf forming the Transformed Atlantic Water (TAW).

During late spring and summer, within the fjord, the Surface Water (SW) forms from glacial meltwaters and this layer can mix with the underlying AW or TAW, forming the Intermediate Water (IW). During autumn and winter, surface water cooling leads to the formation of the Local Water (LW). Sea ice formations and consequent brine releases form cold and dense Winter Cooled Water (WCW). During spring and early summer, LW and WCW progressively warm up and decrease in salinity and so are merged in the IW.

Most of the freshwater inputs into the fjord come from glacier runoff with the major contribution coming from the fjord head (i.e., Kronebreen and Kongsvegen glaciers; Pramanik et al., 2018). Glacier meltwater exits from the bottom of the terminus through subglacial channels forming a buoyant turbulent plume (How et al., 2017). Subglacial runoff and consequent upwelling of meltwater plumes in front of the tidewater glacier front generate a strong surface outflow and consequent sub-surface inflow of warm and saline AW that promotes submarine melting at the glacier front (Cowton et al., 2015; Sundfjord et al., 2017). It was indeed observed that frontal ablation of tidewater glaciers is primarily controlled by warm sub-surface waters (Holmes et al., 2019; Luckman et al., 2015). During summer, the Kronebreen glacier is a main source of meltwaters and suspended particles which consists in a typical glacial upwelling system; this source forms a plume of fresh and turbid meltwaters spreading in the inner part of the fjord (Meslard et al., 2018). The contribution of continental glaciers to the freshwater inputs is not yet fully understood, but the changes observed in the drainage rivers network from the Lovenbreen glaciers (Bourriquen et al., 2018) reveal their important impact related to the glacier retreat.

2.3. Productivity and organic matter export in the Kongsfjorden

In Arctic environments, phytoplanktonic blooms are limited by light availability and sea ice cover. Spring blooms occur after sea ice break-up and consequent light availability increase, but their timing and intensity can change yearly (Hegseth and Tverberg, 2013; Hodal et al., 2012). Also, changes in community structure in relation to water mass advection from the Fram Strait into the fjord were observed for phytoplankton (Hegseth and Tverberg, 2013; Hodal et al., 2012; Lalande et al., 2016; Piquet et al., 2014). During spring, export fluxes of biogenic matter (phytoplankton) are controlled by zooplankton grazing and sink processes (Lalande et al., 2016).

In the summer season, freshwater inputs from land-terminating glaciers do not seem to affect the euphotic depth, whereas meltwater discharges from marine-terminating glaciers have demonstrated a negative impact on the light penetration depth (Payne and Roesler, 2019). Meltwater plumes scatter high quantity of suspended matter away from the glacier front which hampers primary productivity (Hopwood et al., 2020) and increases benthic deposition processes via flocculation at the glacier fronts (Halbach et al., 2019; Payne and Roesler, 2019).

Although export fluxes of matter are reduced to high input of inorganic particles from glaciers particularly in the innermost part of the fjord (Lalande et al., 2016), meltwater turbid plumes have a fundamental role in fjord ecosystems. Surface waters are continuously supplied by meltwater at the tidewater glacier fronts and are pushed away from the coast and replaced by intermediate water rich in plankton and nutrients from the outer fjord (Lydersen et al., 2014). This upwelling system promotes the formation of foraging area (for seabirds and marine mammals) identified as “ecological hotspots” (Lydersen et al., 2014). Furthermore, water masses advected from the shelf carry Arctic and Atlantic faunas (Basedow et al., 2004; Willis et al., 2006), influencing fjord’s biodiversity.

3. Material and methods

3.1 Environmental parameters

3.1.1 CTD (conductivity-temperature-depth) profiles

In August 2018, several water column casts were performed with a conductivity-temperature-depth sensor (CTD profiler, Saiv SD204) equipped with a fluorometer. We selected ten CTD casts (Table 1) close to the sediment sampling stations (see Fig. 2a) to determine water masses characteristics at the sampling time.

The Ocean Data View software V.5.3.0 (ODV, Schlitzer, 2020) was used to produce temperature and salinity plots. Mean surface turbidity was calculated considering the uppermost 20 m of the surface column, then an interpolation plot was performed with inverse distance weighted interpolation using the function *interpolate_spatial* in the R package PlotSvalbard (Vihtakari, 2020).

Station	Transect line	Sampling date	Latitude (N)	Longitude (E)	Max depth (m)
CTD1	**Proximal**	21/08/2018	78°52.769'	12°29.809'	72.3
CTD2	**Proximal**	21/08/2018	78°53.353'	12°29.368'	67.9
CTD3	**Proximal**	21/08/2018	78°53.159'	12°25.378'	85
CTD4	**Proximal**	23/08/2018	78°53.413'	12°25.045'	38.7
CTD5	**Proximal**	21/08/2018	78°54.272'	12°26.560'	64
CTD6	**Medial**	21/08/2018	78°54.122'	12°15.771'	33.8
CTD7	**Medial**	21/08/2018	78°54.873'	12°14.641'	104
CTD8	**Medial**	21/08/2018	78°54.717'	12°11.992'	86.3
CTD9	**Distal**	21/08/2018	78°55.104'	12°7.082'	138
CTD10	**Distal**	21/08/2018	78°56.221'	12°9.760'	142

Table 1. Sampling date and degrees decimal minutes coordinates of the ten CTD cast location during the ISMOGLAC mission.

3.1.2 Sediment sampling

In the frame of the IPEV field campaign C3 (Coasts under Climat Change suite) organised in August 2018, within a collaboration with the Aztec Lady sailing boat, the KING18 mission allowed to sample nine stations along a SE-NW transect in the Kongsfjorden, from about 2 km to 12 km off the Kronebreen and Kongsvegen tidewater glacier fronts (Table 2, Fig. 1). The order of the stations is reported based on the distance from the glacier front, determining three

zone along the studied transect, i.e. proximal stations close to the glacier front margin, medial stations located in a ~75m-deep sub-basin (enclosed in shoals and small islands), and distal stations, at the fjord trench head, deeper than 100 meters. The sediment-water interface was properly sampled by use of a GeMAX corer that collected two twin sediment cores (9 cm inner diameter) at each station: the first for grain size and organic matter analyses and the second for foraminiferal analyses.

Station	Transect line	Sampling date	Latitude (N)	Longitude (E)	Sampling depth (m)	Distance from the front (km)
St2	**Proximal**	21/08/2018	78°53.053'	12°30.780'	49	1.92
St7	**Proximal**	22/08/2018	78°54.239'	12°26.142'	68	4.53
St1	**Medial**	21/08/2018	78°53.847'	12°19.520'	52	6.22
St3	**Medial**	21/08/2018	78°53.705'	12°15.006'	38	7.68
St4	**Medial**	22/08/2018	78°53.905'	12°13.657'	35.5	8.25
St5	**Medial**	22/08/2018	78°54.382'	12°14.511'	75.7	8.25
St8	**Distal**	22/08/2018	78°54.966'	12°06.917'	114	11.18
St6	**Distal**	22/08/2018	78°56.241'	12°09.806'	148	11.43
St9	**Distal**	22/08/2018	78°55.447'	12°04.086'	156	12.47

Table 2. Location along the transect, sampling date, degrees decimal minutes coordinates, sampling water depth and distance from the glacier front of the nine stations sampled during the KING18 mission.

3.1.3 Sediment grain size and carbon analysis

At each station, one core was sliced on board, collecting seven sediment layers (every 0.5 cm between 0 and 2 cm and every 1 cm from 2 down to 5 cm depth, i.e., 0–0.5, 0.5–1, 1–1.5, 1.5-2, 2-3, 3-4 and 4-5 cm), then stored at +4°C. In the laboratory, an aliquot of each slice was used for grain size analyses and the rest was lyophilised for carbon analyses. The laser diffraction particle size analyser Malvern Mastersizer 3000 was used to obtain grain size data. The particle size distributions were analysed with GRADISTAT 8.0 software program (Blott and Pye, 2001).

The carbon analysis was performed using a TOC-V_{CPH} analyser. This instrument measures the free CO_2 gas released by the combustion of the carbon contained in the sediment sample

using a non-dispersive infrared system (NDIR). The total carbon (TC) and total inorganic carbon (TIC) contents were determined on three pseudo-replicates and their values were calculated based on two calibration curves using two standards (glucose for TC and sodium bicarbonate for TIC). The combustion at 900°C of 100 mg of sediment has been used to determine the TC. The combustion at 200°C of 100 mg of sediment was conducted after the addition of 450 µl of concentrate phosphoric acid to determine the TIC. The total organic carbon (TOC) was then calculated indirectly as the difference between the TC and the TIC (Bisutti et al., 2004).

3.1.4 Correlation among environmental variables

Pearson correlations and two sided test between environmental variables were calculated and illustrated using the *ggpairs* function in the R package *GGally* (Schloerke et al., 2021). The correlations were tested for sediment-related properties measured in the 0-0.5 cm sediment layer (i.e., percentage of total carbon (TC), percentage of total inorganic carbon (TIC), percentage of total organic carbon (TOC), percentage of sand, silt and clay), sampling water depth (expressed in meters), extrapolated mean surface water turbidity (0-20 m, expressed in FTU), and distance from the glacier front (expressed in kilometers).

Mean surface water turbidity was extrapolated for sediment sampling coordinates performing inverse distance weighted interpolation on CTD cast measurements using the function *interpolate_spatial* in the R package *PlotSvalbard* (Vihtakari, 2020).

The distance of each sampling station from the front of the glacier was calculate as follow. We used the satellite image taken on the 1st of August 2018 by LANDSAT7 and LANDSAT8 (https://landsatlook.usgs.gov) as a reference for the position of the Kronebreen glacier front at

the sampling time. Then, the reference point for the front position was selected along the centre-line of the glacier (calculated using the box method; Lea et al., 2014) and its coordinates (i.e., 78°52'39.19"N, 12°35'42.51"E) were obtained using the Google Earth Pro software V 7.3.3.7786 (https://www.google.com/earth/index.html) after overlying the satellite image. The distances between the reference point and the individual sampling stations were calculated using the *distm* and *distGeo* functions in the R package *geosphere* (Hijmans, 2019).

3.2 Foraminiferal analyses

3.2.1 Sample processing

Immediately after recovery, the interface cores were sliced horizontally as for the sedimentary analysis (every 0.5 cm between 0 and 2 cm and every 1 cm from 2 down to 5 cm depth, i.e. 0–0.5, 0.5–1, 1–1.5, 1.5-2, 2-3, 3-4 and 4-5 cm). Following the FOBIMO recommendations (Schönfeld et al., 2012), each sample was stored in a 500 cm^3 bottle filled with 95% ethanol with 2 $g.L^{-1}$ of rose bengal stain (to label living foraminifera). In the laboratory, sediment samples were sieved through 63 and 150 µm meshes, then stored in 95% ethanol. All living (rose bengal-stained) specimens of the >150 µm fraction were hand-picked in water for each sediment layer. The small fraction 63-150 µm was considered to investigate potential supplementary ecological information (i.e., presence of juveniles, elongated and/or small sized species), knowing that high densities of small sized foraminifera are common in foraminiferal studies (e.g., Duchemin et al., 2007; Shepherd et al., 2007; Gooday and Goineau, 2019; Fossile et al., 2020). However, being extremely time-consuming, the picking of the living foraminifera from the 63-150 µm size fraction was restricted to the uppermost centimetre of

331 the sediment. Due to high foraminiferal abundances, some samples of the small fraction were
332 dried at 50°C, split with an Otto Microsplitter and hand-sorted to reach a minimum of 300
333 individuals from a whole subsample, then standardised to the entire sample.

334 The presence of fragments of living and dead specimens of two large tubular agglutinated
335 species (*Hyperammina sp.* and *Archimerismus subnodosus*) was documented in some
336 samples (St5, St6, St8 and St9). However, due to the fragility of their test and impossibility to
337 determine the number of individuals represented by the observed fragments, they were not
338 included in the quantitative analysis (e.g., Duros et al., 2013; Caulle et al., 2014). Scanning
339 electron micrographs (SEM) of the major agglutinated and calcareous species are shown in
340 Plate 1 and Plate 2, respectively. *Cassidulina* spp. and *Islandiella* spp. SEM and
341 stereomicroscope pictures are displayed in Figure S4.

342 The dead assemblages from 4-5 cm were picked and analysed to highlight possible
343 differences between living and dead assemblages due to seasonal variability. To do so, the
344 L/(L+D) ratios (%Living / (%Living + %Dead); (Jorissen et al., 1998) were calculated
345 considering the living assemblages from the 0-5 cm core top interval (merging the seven
346 sediment layers) and the dead assemblages from the 4-5 cm sediment layer, for all species >
347 5% in either living or dead assemblages. A ratio ranging between 0 and 0.5 indicates that a
348 species is relatively more abundant in the dead fauna, whereas a species is more abundant in
349 the living assemblage when the ratio ranges between 0.5 and 1. A species is equally abundant
350 in the living and dead assemblages when the ratio is 0.5. As it was not possible to calculate
351 the accumulation rates at our sampling stations, we cannot ascertain whether the 4-5 cm layer
352 a good representation of the thaphonomic loss. Therefore, the L/(L+D) ratios were only used

353 to have a qualitative information on possible seasonal sampling bias. A ratio of 0.5 indicates
354 that there is no discrepancy between the relative abundance of the given species sampled
355 alive in August 2018 and its production all year along. Higher or lower ratios suggest that the
356 sampling time (i.e., August 2018) is not representative of the given species life cycle.

357 *3.2.2 Diversity metrics and multivariate analysis*

358 Taxonomic diversity was estimated using three different metrics using R package *vegan*
359 (Oksanen, 2019):

360 1. Species richness (S; i.e., number of species);

361 2. Shannon–Wiener Index (H') calculated as:

$$H' = -\sum_{i=1}^{S} p_i \ln p_i \quad \text{(i)}$$

362 where p_i is the proportion of each species i in the community;

363 3. Pielou's evenness (J) calculated as:

$$J = \frac{H'}{\ln S} \quad \text{(ii)}$$

364

365 All multivariate analyses were performed using the R software (v. 4.0.0; R Core Team,
366 2020). Hierarchical clustering analyses were performed on relative abundances considering
367 the 0-5 cm sediment layer and the >150 µm size fraction (Bray-Curtis dissimilarity measure).
368 The cluster on stations (complete linkage method) was performed on foraminiferal densities
369 considering all the species, whereas the cluster on the species (average linkage method) used
370 only the densities of the major species (relative abundance >5%). Dissimilarity matrices were

371 calculated using the *vegdist* function in the R package *vegan* (Oksanen, 2019). Different
372 linkage methods were compared among each other and cophenetic distances were computed
373 to assess clustering consistency. Dendrograms were produced with *fviz_dend* function in the
374 R package *factoextra* (Kassambara and Mundt, 2020).

375 Transformation-based redundancy analysis (tb-RDA) was performed on living foraminiferal
376 community considering the 0-5 cm sediment layer and the >150 µm size fraction in relation to
377 environmental parameters. Forward selection was performed on several environmental
378 variables (bottom water depth, TOC, sand, silt, clay percentages and surface water turbidity)
379 and only three parameters were retained (i.e., turbidity and depth, $p < 0.05$; TOC, $p < 0.1$). The
380 significance of the model and ordination axes was tested with the *anova.cca* function in the R
381 package *vegan* (Oksanen, 2019), applying Bonferroni correction. Hellinger transformation was
382 applied to foraminiferal densities, whereas environmental variables were centred and scaled.
383 Both transformations were performed using the *decostand* function in the R package *vegan*
384 (Oksanen, 2019). Adjusted R^2 was calculated to determine the model fit.

385 Differences between the two size fractions (63-150 µm and >150 µm) in the 0-1 cm
386 sediment layer were investigated with a non-metric multidimensional scaling analysis (nMDS).
387 The analysis was performed on foraminiferal densities using the *metaMDS* function (which
388 applied square root transformation and wisconsin double standardisation) in the R package
389 *vegan* (Oksanen, 2019) using Bray-Curtis dissimilarity. A similarity of percentages (SIMPER)
390 analysis was performed using the *simper* function in R package *vegan* (Oksanen, 2019) to
391 investigate the relative contribution of each species to the difference between size fractions.

The most influential species (i.e., $p<0.01$ and average contribution >5%) were extracted and displayed on the nMDS biplot.

4. Results

4.1 Environmental parameters

4.1.1 Water properties

During August 2018, a water stratification was well established in the Kongsfjorden (Fig. 2). All over the inner fjord, the uppermost 10 m of the water column were relatively fresh (salinity range = 30.0 - 34.0) with a narrow temperature range between 3.5 and 4.0°C. This upper layer can be defined as Surface Water (SW, T>1°C and S<34.0; Cottier et al., 2005) supplied by intense ice melting during summer. In the 4-10 km section of the sampling transect, waters with the highest temperature, between 4.5 and 5.5°C, and a narrow salinity range (S=34.7-34.9) were detected below the Surface Water. This relatively warm and saline water mass extending from 10 m to about 30 m water depth was less distinguishable in the innermost part of the fjord. It can be identified as Atlantic Water (AW, T>3°C and S>34.65; Cottier et al., 2005) intruding into the fjord up to at least 4 km from the Kronebreen-Kongsvegen glacial front. Below 50m depth in 4-10 km section of the transect, the homogeneous water column (T=3-4°C, S=34.7-34.9) can be described as Intermediate Water (IW, T>1°C and 34.00<S<34.65; Cottier et al., 2005) resulting from the year round mixing of the AW with the SW. In the innermost part of the fjord (0-4 km of the section transect), a cold layer of 1.5 to 3.0°C appeared at the bottom, likely issued from subglacial discharges flowing at the glacier front. The water stratification

observed in the Kongsfjorden in August 2018, due to freshwater input from glacial melting and AW inflow, is typical of the summer season (as described by Svendsen et al., 2002).

The surface water turbidity (average of the 0-20 m layer) displayed values above 80 FTU in front of the Kronebreen-Kongsvegen terminus and below 20 FTU in all stations located close to the southern coast or far away from the glacier front (Fig. S1).

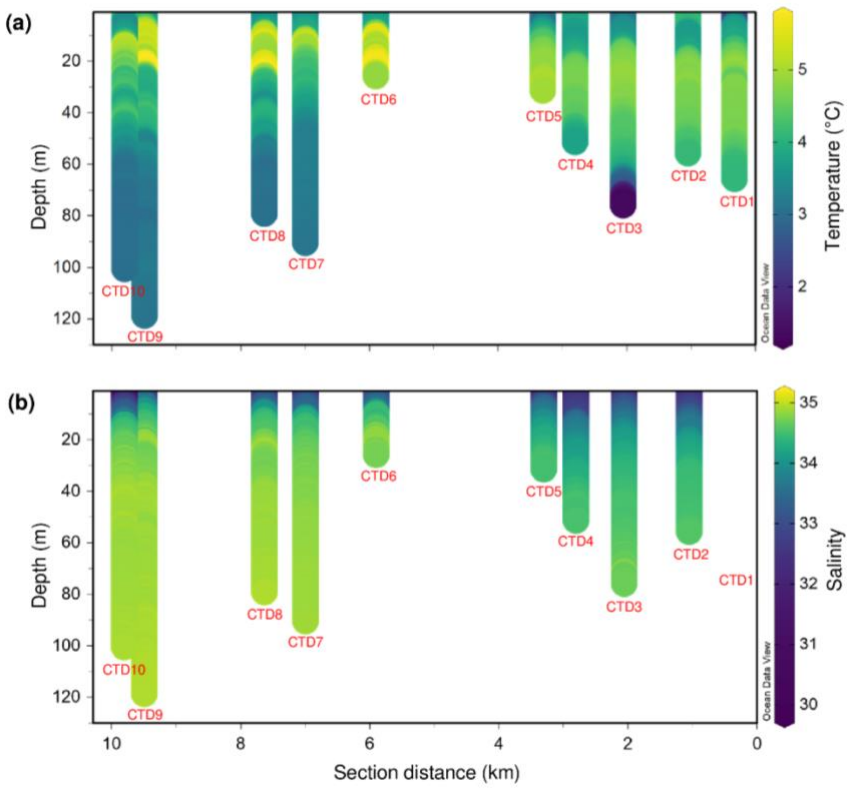

Figure 2. SE-NW 0-130 m deep sections across the Kongsfjorden of the 10 CTD casts for temperature (°C) **(a)** and salinity **(b)**. Salinity data for CTD1 are not available.

4.1.2 Grain size analyses

Sediments, at all stations and both surficial (0-0.5 cm) and intermediate (2-3 cm) levels, were medium silts with mean grain sizes ranging from 6.3 to 16.3 µm (Table S1). Grain size curves mainly showed unimodal distribution with a single mode around 7-9 µm, except at the 2-3 cm level from two stations (St2 and St8) where a second mode picks at 37.7 and 62.9 µm

426 respectively, indicating a mixture with a population of coarse silts. At all stations, the mean
427 values slightly increased with depth, a trend more obvious at St2 and St8 (coherent with the
428 bimodal distribution mentioned above), and at the two shallowest stations close to the southern
429 coast of the fjord (St3 and St4) where the single mode reached 17.5 and 22.6 µm, respectively.
430 At all stations, the percentage of sand (>63 µm) remained low, about or below 10%, except at
431 depth at St8 where it reached almost 20% (coherent with the secondary mode of the grainsize
432 distribution at 62.9 µm). The percentage of clay (<2 µm) was everywhere slightly higher in the
433 surficial sediments and ranging from around 10 to 18%.

434 *4.1.3 Organic matter analysis*

435 All the sampled stations were characterised by total carbon contents (TC%) between 2.68 and
436 3.10% in the surface sediment layer (0-0.5 cm) (Table 4). TC was mostly composed of
437 inorganic carbon (TIC%; values between 2.07 and 2.65 %). Therefore, the total organic carbon
438 content (TOC%) of the fjord showed values below 0.70% at all stations (Table 3). In general,
439 TOC percentages were lower close to the terminus in the innermost fjord (St2, St7 and St1
440 <0.40%) than at downstream stations (between 0.40 and 0.70%). TOC percentages are
441 significantly different among the stations (One-Way ANOVA, $p<0.001$) (Table 3).

Stations	Location	TC	TIC	TOC
St2	**Proximal**	2.78±0.03	2.59±0.07	0.20±0.04
St7	**Proximal**	2.84±0.05	2.44±0.05	0.40±0.04
St1	**Medial**	2.78±0.01	2.65±0.02	0.12±0.01
St3	**Medial**	2.75±0.03	2.26±0.08	0.48±0.05
St4	**Medial**	2.68±0.02	2.30±0.04	0.38±0.03
St5	**Medial**	3.10±0.01	2.40±0.07	0.70±0.04
St8	**Distal**	2.76±0.05	2.28±0.01	0.48±0.03
St6	**Distal**	3.04±0.03	2.39±0.02	0.65±0.02
St9	**Distal**	2.73±0.02	2.07±0.03	0.65±0.02

Table 3. Total carbon (TC), Total Inorganic Carbon (TIC) and Total Organic Carbon (TOC) percentages measured on the uppermost sediment layer (0-0.5 cm) at each sampling station. Data are displayed as mean ± standard deviation (n=3).

4.1.4 Correlation between environmental variables

Few significant relationships were observed between environmental variables (Fig. S2). The most significant correlations were observed between distance from the glacier front and turbidity of surface waters ($r = -0.969$, $p<0.001$) and between sampling depth and sediment clay percentage ($r = -0.90$, $p<0.001$). Distance from the front was also significantly correlated with TIC and TOC percentages in sediment ($r = -0.739$, 0.729, respectively, $p<0.05$).

4.2 Foraminiferal assemblages in the upper 5 cm sediment (>150 µm fraction)

4.2.1 Abundances and diversity

Foraminiferal absolute densities and diversity metrics, considering the 0-5 cm sediment interval and the >150 fraction, are displayed in Table 4. Abundances were below 300 ind. 50 cm^{-2} in the three stations closest to the glacial front (proximal stations St2 and St7 and the first medial station St1). The other medial and distal stations located beyond 6 km from the terminus showed abundances between 1700 and 3500 ind. 50 cm^{-2} (except St4 with 658 ind. 50 cm^{-2}). The number of species was about or below 10 in the innermost proximal stations (St2 and St7) and almost double at the first medial station (St1), whereas all the other stations showed a species richness between 32 and 49. Low values of Shannon-Wiener Index H' were found at the proximal stations (below 1), a small increase in diversity was observed at St3, St6 and St8 (values between 1 and 2), whereas higher H' values (above 2) were observed at St1, St4, St5 and St9. The equitability (J, Table 4) was below 0.50 at St2, St3, St7 and St8, whereas higher values (up to 0.73) were observed at the other locations.

Stations	Transect location	Density (ind. 50cm^{-2})	Richness (S)	Shannon-Wiener (H')	Equitability (J)
St2	**Proximal**	261	8	0.91	0.44
St7	**Proximal**	238	10	0.99	0.43
St1	**Medial**	263	19	2.16	0.73
St3	**Medial**	2308	34	1.12	0.32

St4	**Medial**	658	36	2.60	0.73
St5	**Medial**	1733	45	2.45	0.64
St8	**Distal**	3485	49	1.78	0.46
St6	**Distal**	1841	43	1.97	0.52
St9	**Distal**	2086	32	2.10	0.61

Table 4. Foraminiferal total abundances (in number of individuals per 50 cm^2) and diversity metrics (richness, equitability and Shannon-Wiener index), considering the total living fauna (>150 µm size fraction) in the 0 to 5 cm core top sediment.

4.2.2 Assemblage composition

The first cluster analysis divided the sampling stations into four clusters: cluster 1 composed by the proximal stations (St2 and St7), cluster 2 including only the first medial St1, cluster 3 grouping the remaining medial stations (St3, St4, and St5) and cluster 4 for the distal stations (St8, St6, and St9) (Fig. 3). The second cluster analysis, performed on the most abundant species only, divided the species in two major groups: group *a* including species present in the proximal stations and first medial station, and group *b* including species present mostly in the other medial and distal stations (Fig. 3).

Foraminiferal species composition in terms of relative abundances is shown in Figure 3 and scanning electron micrographs (SEM) of the major species are displayed in Plate 1 and 2. The proximal station St2 was dominated by the agglutinated *Capsammina bowmanni* (73%) and *Saccammina* cf. *sphaerica* (15%), with a minor contribution from the miliolid *Quinqueloculina stalkeri*. *Capsammina bowmanni* was also dominant at the other proximal station St7 (55%), together with the calcareous *Cassidulina reniforme* (39%). *Cassidulina reniforme*, *Nonionellina labradorica*, *Reophax fusiformis* and *Textularia earlandi* were the main species at the medial St1 with abundances between 15 and 20%. The medial St3 assemblage was characterised by *Nonionellina labradorica* (78%), which was also a major component in the medial and distal stations (with abundances between 13 and 33 %). *Globobulimina auriculata* made up to 13% at St4. The agglutinated *Adercotryma glomeratum* showed high relative abundances (between 35 and 57%) at the distal stations (St8, St6, St9). *Cibicidoides lobatulus* reached the 11% only in the outermost station St9.

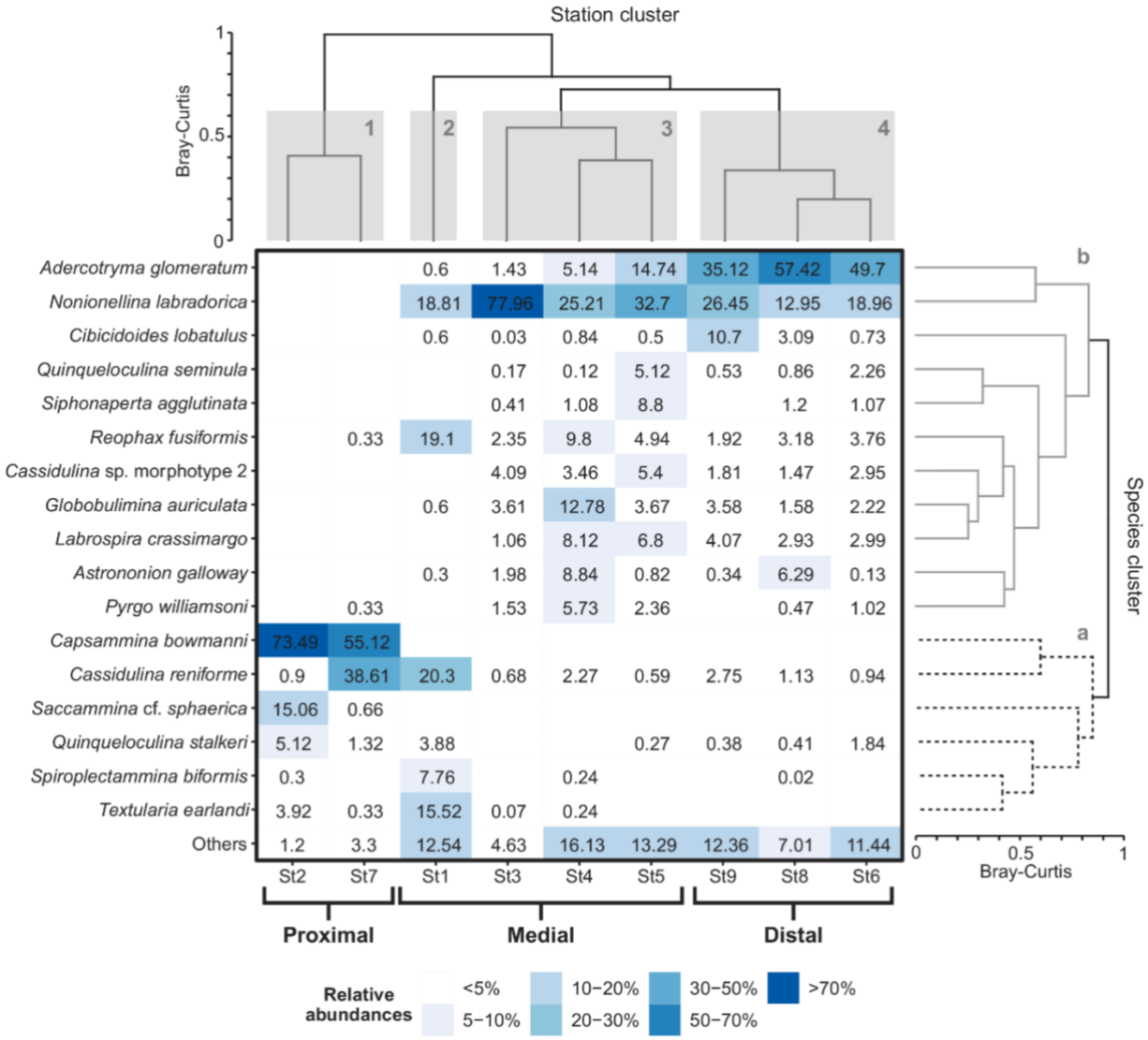

Figure 3. Heatmap showing the cluster analysis of the foraminiferal fauna based on relative abundances of the major species considering the total living faunas (>150µm size fraction) in the 0 to 5 cm core top sediment. The dichotomy clustering is based on the Bray-Curtis dissimilarity. The station cluster (complete linkage method) considers all the species whereas the species cluster (average linkage method) considers only the relative abundances of the major species (>5 %).

4.2.3 Microhabitat distribution

The foraminiferal vertical distribution profiles from the surface down to 5 cm sediment depth were heterogeneous along the fjord axis (Fig. 4). Living foraminifera were present mostly in the uppermost half centimetre of sediment, rapidly disappearing downcore at the two proximal stations (St2 and St7; cluster 1). This surface layer was dominated by *C. bowmanni* and

Saccamina cf *sphaerica* at St2, whereas St7 was characterised by *C. bowmanni* and *C. reniforme*. Cluster 2 including only St1 shows the presence of *C. reniforme* mostly in the 0-0.5 cm layer together with other species (e.g., *N. labradorica*, *R. fusiformis* and *T. earlandi*). The three medial stations of cluster 3 (St3, St4, St5) showed the typical exponential decrease in foraminiferal density with sediment depth. Some species were mostly present in the uppermost centimetre (e.g., *Cassidulina* sp. morphotype 2 and *Labrospira crassimargo*). The only species abundant below the 0-0.5 cm layer were *N. labradorica*, particularly at St3, and *Globobulimina auriculata*, even more abundant at the 1-2 cm layer of St4. In the distal stations (cluster 4), deep infauna (i.e., *A. glomeratum* and/or *N. labradorica*) was encountered. Foraminiferal densities at St6 remained similar at all layers below the 0.5 cm depth. On the contrary St9 showed a subsurface peak at 1-2 cm depth with foraminiferal density almost double than the uppermost centimetre due to the high density of *A. glomeratum* and *N. labradorica*. The intermediate and deep infaunal microhabitats showed similar species compositions than the uppermost centimetre.

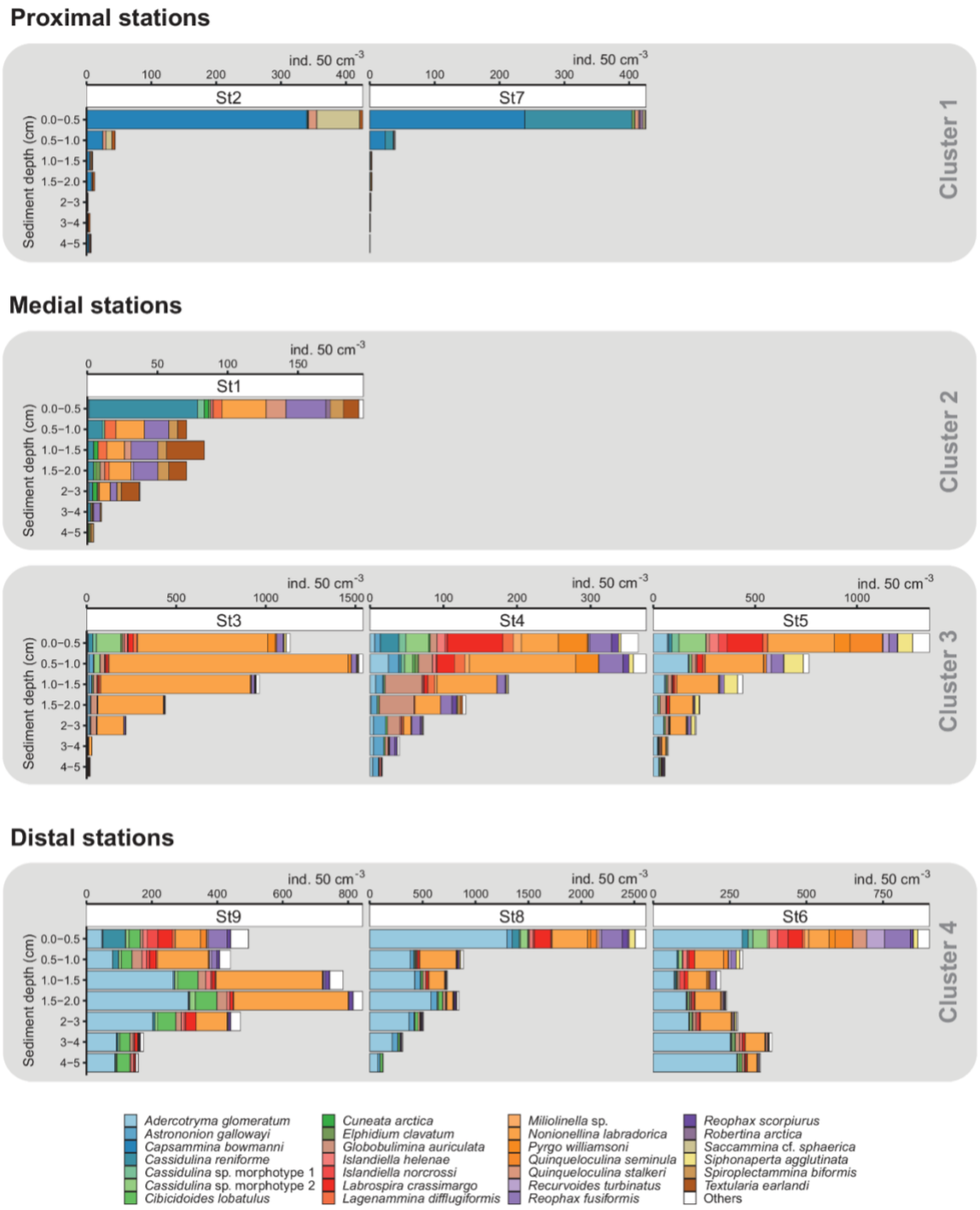

Figure 4. Foraminiferal microhabitat distribution of the most representative species (contributing with >5% in at least one sample) from the sediment surface down to 5 cm depth considering the >150 µm fraction. Note that stations are displayed based on their location (proximal, medial, distal) and on the results of the station cluster analysis displayed in Fig. 3.

4.2.3 Redundancy analysis

Three predictors of variation in species composition were identified from the redundancy analysis (turbidity and depth $p<0.05$; TOC, $p<0.1$). The first two components of the model explained 66.4% of the total variance (r^2 adjusted = 0.59). RDA1 was positively correlated with sediment organic matter content (TOC) and water depth, and negatively with surface water turbidity. Opposite correlations were observed for the RDA2. RDA1 separates the proximal stations plus St1 from the other medial and distal stations. RDA2 separates proximal and distal stations from the medial stations. The proximal stations were positively correlated with turbidity, whereas the distal stations with TOC and depth. The three species with the highest scores are *C. bowmanni*, *N. labradorica* and *A. glomeratum*, which were the major species respectively at the proximal, medial and distal stations.

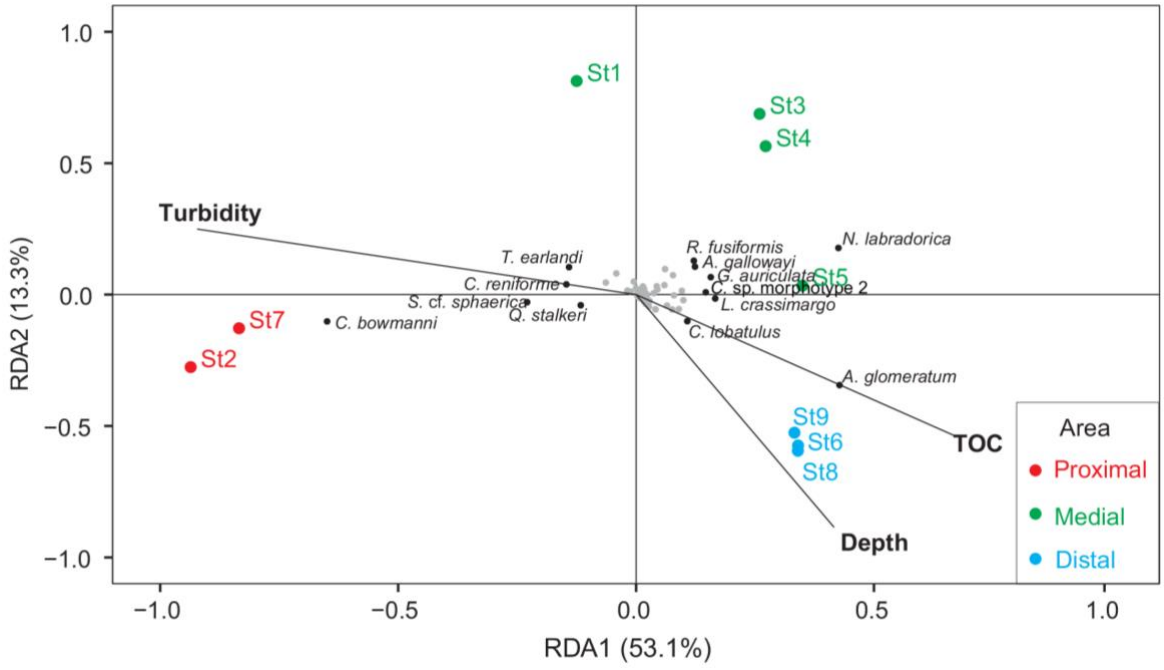

Figure 5. Transformed-based redundancy analysis (tb-RDA) performed on living foraminiferal community (total densities in the 0-5 cm interval, >150 µm fraction) in relation to three significative environmental parameters (surface water turbidity in the 0-20 m surface layer, percentage of TOC, and sampling water depth).

4.3 Comparison between the 63-150 µm and > 150 µm size fractions (in the 1 cm core top)

4.3.1 Abundance and diversity

Foraminiferal densities and diversity metrics were calculated considering the 63-150 µm and >150 µm fractions in the 0-1 cm sediment layer (Fig. 6). The finer fraction (63-150 µm) showed abundances always higher than the coarse fraction (>150 µm) with densities between 1000 and 4700 ind. 50 cm^{-2}. The small fraction contributed from 72 up to 96% to the total densities (63-150 µm + >150 µm) (Fig. 6a). Foraminiferal densities considering the >150 µm were lower than 300 ind. 50 cm^{-2} at St2, St7 and St1, between 300 and 600 ind.50cm^{-2} at St4, St6 and St9 and over 1000 ind.50cm^{-2} at St3, St5 and St8.

Less than 20 species were observed for both size fractions in the first three stations of the transect (St2, St7 and St1), whereas values between 29 and 57 were observed further away in the transect. The number of species observed in the finer fraction was always higher than in the coarse fraction but with a similar trend along the main fjord axis (Fig.6b).

Shannon-Wiener index was lower than 2 at the three innermost stations, whereas values between 2 and 3 were observed further away in the transect considering the finer fraction (63-150 µm). The >150 fraction presented values lower than 1.5 at the station St2, St7 and St3, values around 2 at St1 and St8, while the remaining stations showed values around 2.5. Equitability values for the >150 µm fraction were below 0.5 at St2, St7 and St3, whereas values between 0.5 and 0.8 were observed at all other stations. The finer fraction (63-150 µm) showed very low equitability at St2, values between 0.5 and 0.6 at St7, St1, and St3, and over 0.7 at the other stations. Shannon-Wiener and equitability diversity metrics showed more variability between the two size assemblages (Fig. 6c, d) compared to species richness (Fig. 6a), but a similar diversity increase from the inner to the outer stations was observed.

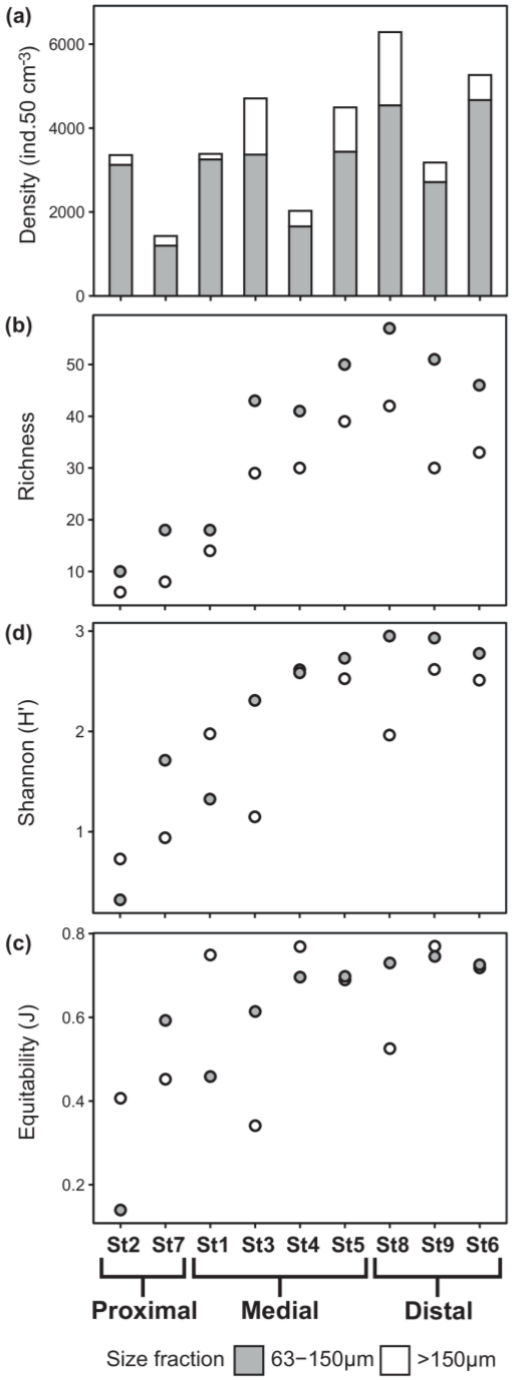

560

561 **Figure 6. (a)** Foraminiferal cumulative densities (ind. 50 cm^{-3}) for two size fractions (63-150 µm > 150
562 µm) of the 0-1 cm sediment layer. **(b)** Shannon-Wiener (H') and **(c)** equitability **(J)** indexes comparison
563 among the 63–150 µm and >150µm fractions. The >150 µm fraction is represented in dark grey and the
564 63-150 µm in light grey.

565 *4.3.2 Non-metric multidimensional scaling analysis*

566 The nMDS ordination plot (stress = 0.071), based on species densities considering the fine
567 (63-150 µm) and coarse (>150 µm) size fractions in the 0-1 cm sediment layer, showed a

similar clustering of the stations by area (proximal, medial, distal) but differences in assemblage composition (Fig. 7). The NMDS1 axis separates the first three stations of the transect (St2, St7, and St1) from the remaining stations, whereas NMDS2 separates the two size fractions. The area of the polygon for the >150 µm size fraction is bigger than the one for the 63-150 µm, indicating lower dissimilarity among stations in the finer fraction.

Although both fractions separated the nine stations into the same stations' clusters, no overlap can be observed between convex hulls due to large differences in foraminiferal assemblages (Fig. 7). Indeed, the SIMPER analysis identified five major species (i.e., *Cassodulina reniforme*, *Textularia earlandi*, *Spiroplectammina biformis*, *Stainforthia feylingi*, *Pullenia* cf. *osloensis*) influencing this difference (average contribution >5%, p<0.01). Four of them were positively correlated with the NMDS2 axis and mostly represented in the 63-150 µm fraction. The only exception being *C. reniforme,* which was almost equally present in both fractions. The two size fractions had 50 common species. The >150 µm had 14 exclusive species, whereas the 63-150 µm presented 21 exclusive species. Species relative abundances for both size fractions are displayed as heatmaps in the supplement (Fig. S3).

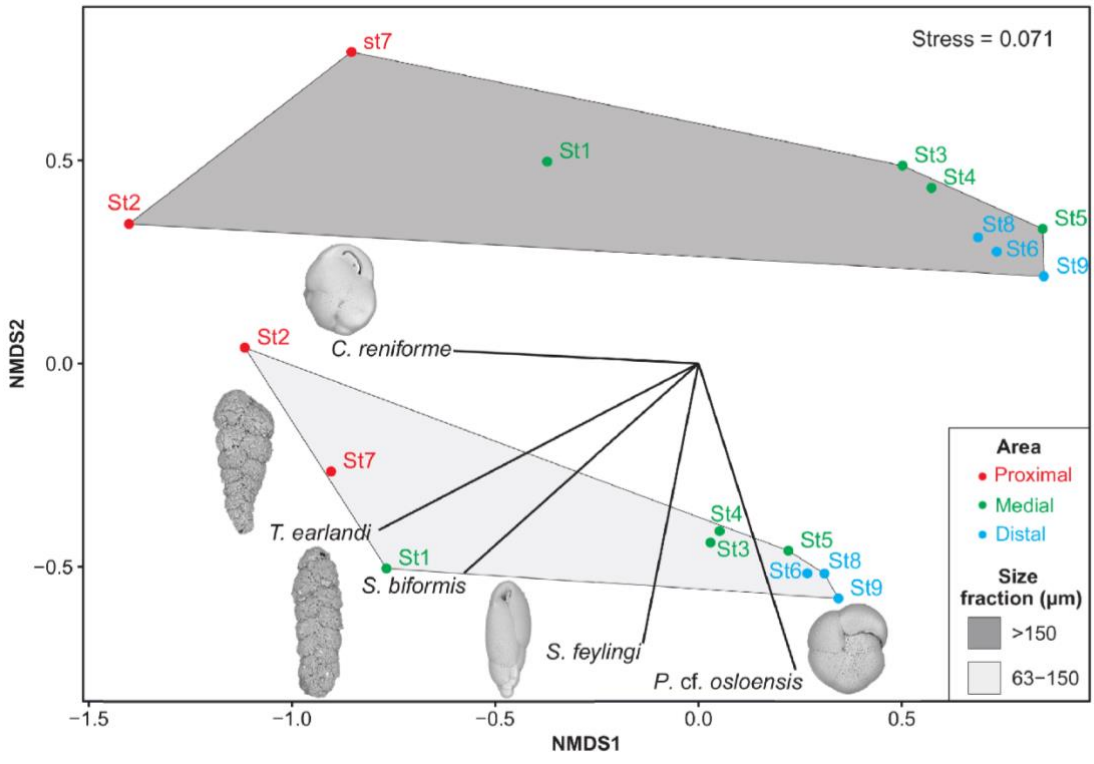

584 **Figure 7.** Non-metric multidimensional scaling (nMDS) analysis (Bray-Curtis dissimilarity) on
585 foraminiferal densities considering two groups corresponding to the two size fractions (63-150 µm and
586 >150 µm) in the 0-1 cm. Station colours correspond to the sampling area (proximal, medial, distal). The
587 convex hulls enclosed each of the groups. The displayed vectors are the species explaining significant
588 ($p<0.01$) percentage of dissimilarity (>5%) between the two groups based on SIMPER analysis.

589 **5. Discussion**

590 The geographical position of Kongsfjorden and its geometric configuration (i.e., no entrance
591 sill) are responsible for the built-up of steep environmental gradients developing along the short
592 fjord axis between two contrasted end-members (Lalande et al., 2016; Meslard et al., 2018;
593 Svendsen et al., 2002). Gradients of water salinity and temperature, turbidity, nutrient
594 distribution, and inorganic particulate sedimentation, are determined by the concomitance of
595 glacier dynamics at the fjord head with the AW inflow from the outer shelf. The present study,
596 performed in August 2018, shows that benthic foraminiferal faunas respond clearly to these
597 summer environmental gradients. Our analyses identified three biozones related to the glacier
598 front in the inner Kongsfjorden: distal, medial and proximal.

599 *I. Proximal biozone*

600 During August 2018, CTD casts detected a water column typical of the summer stratification
601 (Svendsen et al, 2002; Cottier et al. 2005) with a fresh surface layer of meltwaters overlying
602 saltier water mass (due to mixing with AW) (Fig. 1). The surface layer also revealed high
603 turbidity, particularly in the vicinity of the front of the tidewater glacier Kronebreen (Fig. S2).
604 This observation confirms previous studies that identified the Kronebreen glacier as the major
605 source of meltwater, suspended particles and sediment in the Kongsfjorden (D'Angelo et al.,
606 2018; Meslard et al., 2018; Svendsen et al., 2002; Trusel et al., 2010). Generally, Kronebreen
607 subglacial discharges and associated sediment load eroded from the glacier basement exit
608 from the northernmost part of the glacier front (Meslard et al., 2018; Trusel et al., 2010).
609 Consequently, a buoyant turbid plume is formed at the tidewater glacier front and is pushed
610 away northwards by the downfjord surface circulation at the fjord head (Sundfjord et al., 2017;

611 Torsvik et al., 2019), implying the spreading of the plume above our sampling stations St2 and
612 St7 (Fig. 1). The fine grained particles, transported in suspension in the plume are deposited
613 with a high sediment rate estimated at about 6-9 cm y^{-1} in the vicinity of the Kronebreen front
614 (< 0.5 km) (Trusel et al., 2010). This explains our observations at the proximal stations where
615 unconsolidated and potentially high mobile surface sediment (i.e., low sediment stability) was
616 composed of medium silt. Coarser particles from subglacial discharges, such as coarse silt
617 and fine sand, can also be transported in suspension in the plume during sporadic
618 hydrodynamic events (e.g., accelerated melting period, surge, storm), and then deposited
619 along a decreasing size gradient off the glacier front (Torsvik et al., 2019). This process may
620 be recorded by layers of coarse silts like observed 3 cm downcore at St2.
621 The proximal stations (St2 and St7), grouped into cluster 1 (Fig. 3), were positively
622 correlated with surface water turbidity (Fig. 5). This area, directly subjected to high
623 sedimentation from the meltwater turbid plume was characterised by low foraminiferal
624 abundances and/or low taxonomic diversity in both size fractions (Table 3, Fig. 6). Only few
625 species (i.e., *Capsammina bowmanni, Saccammina* cf *sphaerica, Cassidulina reniforme* and
626 *Textularia earlandi*) that are most likely adapted to colonise soft-bottom sediments subjected
627 to high physical disturbance, were identified in this area (Fig. 3 and Fig. 7). The agglutinated
628 monothalamus species *C. bowmanni* completely dominated the assemblage in the immediate
629 proximity of the glacier (St2, 1.9 km far from the glacier front). This species lives preferentially
630 in the uppermost centimetre of the sediment (Gooday et al., 2010) and was previously reported
631 in a temperate fjord under fluvial influence in southern Norway (e.g., Alve and Nagy, 1986).
632 However, it has never been reported as a dominant species and its presence has not been
633 often documented, likely due to the fragility of the test that can be lost during sample
634 preparation. At St7, *C. bowmanni* was accompanied by *C. reniforme* and *T. earlandi*. The
635 increased distance (about 4.5 km) from the glacier front and a consequent slightly reduced
636 environmental stress may have favoured the coexistence of these species. *Cassidulina*
637 *reniforme* is a typical glacier proximal species that has been previously observed in several
638 Svalbard fjords from the western coast (Adventfjorden, Hornsund, Van Mijenfjorden, Isfjorden,

639 Tempelfjorden, Krossfjorden, Smeerenburgfjorden; Hald and Korsun, 1997; Korsun and Hald,
640 2000; Szymańska et al., 2017) and from the southern coast (Storfjorden; Fossile et al., 2020).
641 This species was suggested to prefer less saline waters (e.g., Hald and Korsun, 1997; Jernas
642 et al., 2018). *Cassidulina reniforme* was also present as juveniles in the fine fraction at the
643 proximal station St7. The presence of juveniles of this glacier-proximal species (e.g., Hald and
644 Korsun, 1997; Korsun and Hald, 1998, 2000) may suggest the opportunistic response to the
645 stressful conditions related to glacier dynamics (i.e., high turbidity and reduced organic flux).
646 In other Svalbard fjords, *C. reniforme* is often accompanied by another glacier proximal
647 opportunist, *Elphidium clavatum* (e.g., Hald and Korsun, 1997; Korsun and Hald, 1998, 2000;
648 Fossile et al., 2020). In the studies mentioned above, it was proposed that *C. reniforme* would
649 replace *E. clavatum* when environmental conditions ameliorate in terms of glacial physical
650 disturbance and food supply. In our study *E. clavatum* was observed only in the dead
651 assemblages, suggesting a potential temporal shift in the dynamics for their reproduction
652 (Table S2). Indeed, high frequencies of *E. clavatum* and *C. reniforme* were documented in
653 September 2015 at the Kongsfjorden head (Kniazeva and Korsun, 2019). In the small size
654 assemblage of St7 there was also the agglutinated *T. earlandi*. This is a typical glaciomarine
655 species usually found in fjord environments (e.g., Korsun and Hald, 2000).
656 The meltwater turbidity plume can spread for several kilometres from the glacier front
657 (Meslard et al., 2018) reducing the euphotic depth to few meters (Halbach et al., 2019) and
658 locally preventing phytoplankton growth. Moreover, glacial runoff transports old and refractory
659 terrestrial organic carbon (Bourgeois et al., 2016; Calleja et al., 2017; Kedra et al., 2012). This
660 generally causes the depletion of available organic matter export fluxes to the seafloor in the
661 inner fjord (Lalande et al., 2016). Previous studies reported sediment depleted in organic
662 carbon close to the Kronebreen terminus (TOC% < 0.25%; Bourgeois et al., 2016).
663 The presence of living foraminifera restricted at the sediment surface (Fig. 4) was likely due
664 to the unconsolidated and potentially mobile sediment (i.e., low sediment stability) caused by
665 rapid accumulation from high suspended sediment load coming from the glacier terminus. But,
666 it can also be a response to the poor TOC concentrations lower or about 0.4% (TROX model,

667 Jorissen et al., 1995). Deposition of massive amounts of sediments can also hamper the
668 oxygen penetration into the sediment. It is well known that oxygen availability as well as organic
669 matter are two limiting factors for foraminiferal microhabitat distribution (Jorissen et al., 1995).
670 Moreover, the presence of *C. bowmanni* and *C. reniforme* restricted at the sediment surface
671 may be the result of their microhabitat preferences. High absolutes and relative densities and
672 microhabitat restriction might be indicative of the pioneer character of *C. bowmanni*. The
673 presence of opportunistic and simple agglutinated species capable of rapid colonisation after
674 physical disturbance was previously observed in highly disturbed areas (i.e., canyons; Koho
675 et al., 2007). This species, together with *T. earlandi* and the calcareous *C. reniforme*, may be
676 the only species able to deal with the stressful conditions prevailing at the sampling time.
677 Similar habitat restrictions to the sediment-water interface were observed for benthic
678 macrofauna in some areas of Arctic fjords subjected to high disturbance (e.g., Wlodarska-
679 Kowalczuk et al., 2005). Finally, the high availability of mica at the Kronebreen terminus
680 originated from mica-schists (from Proterozoic low- and medium-grade metamorphic rocks;
681 Svendsen et al., 2002), could have also played a positive role in the thriving of *C. bowmanni*.
682 Indeed, this species appears to have an obligated use of mica flakes to build its test (Gooday
683 et al., 2010).

684 *II. Medial biozone*

685 In the central part of the inner fjord, the water column was characterised by the same fresh
686 surface layer and a clear signal of AW intrusion (Fig. 1). A reduced water turbidity compared
687 to the proximal area was observed (Fig. S1). The increased distance from the glacier front and
688 a progressive dispersal of the meltwater turbid plume coming from Kronebreen can explain
689 such pattern (e.g., Meslard et al., 2019). Medium silts were also observed in this area, as a
690 result of the sedimentation from the meltwater turbid plume away from the glacier front. Indeed,
691 high sedimentation rates were previously estimated to values of about 2.5 cm yr^{-1} in the medial
692 zone, but they are 2.5 to 3.5 times lower than the ones measured in the proximal zone
693 (Zaborska et al., 2006). At the two shallowest stations St3 and St4, located in front of glacial

694 sandur deltas, in the vicinity of prodeltas (Bourriquen et al., 2016) developed along the
695 southern coast, coarse silts were observed as a secondary peak in the grainsize distribution
696 of down core sediment layers. This relatively coarse particulate input to the fjord may be
697 provided by meltwaters (and associated sedimentary load) derived from the sandur drainage
698 downstream the continental glaciers (i.e., Austre Lovénbreen and Midtre Lovénbreen) located
699 on the southern bank of the fjord (Bourriquen et al., 2018).

700 The medial stations grouped into cluster 2 (St1 alone) and cluster 3 (St3, St4 and St5) (Fig.
701 3) do not show any strong correlation with a specific environmental variable (Fig. 5), but
702 foraminiferal communities showed some differences between the two identified clusters. St1
703 was separated from the remaining medial stations and it was composed by a transitional
704 assemblage from the proximal to the medial biozone, characterised by the presence of *C.*
705 *reniforme*, *Reophax fusiformis* and *T. earlandi*. *Cassidulina reniforme*, which was also
706 dominant in the proximal station assemblages, could indicate the persistence of the tidewater
707 glacier disturbance, as also suggested by the presence of juveniles of this species. Moreover,
708 the relatively high disturbance at St1 is supported by the lowest TOC content (around 0.1 %)
709 measured along the transect. *Textularia earlandi*, was the dominant species in the small size
710 assemblage of St1. This elongated species together with *Spiroplectammina biformis* was
711 mostly present in the fine fraction and especially in the medial stations (Fig. 7, Fig. S3). Both
712 species are typical of glaciomarine environments, and their relative abundances usually
713 increase with distance from the glacier but still under glacier influence (e.g., Korsun and Hald,
714 2000; Forwick et al., 2010; Szymańska et al., 2017; Fossile et al., 2020). The agglutinated *R.*
715 *fusiformis* was previously observed together with *T. earlandi*, in a West Greenland fjord, an
716 Arctic fjord under the influence of Atlantic-sourced waters (Lloyd, 2006). The preference of
717 both species for these waters is coherent with their presence in August 2018 when an AW
718 intrusion was clearly observed in the medial area. Station St1 presented also high relative
719 abundances of *Nonionellina labradorica*, which is in common with all the other medial stations
720 grouped into cluster 3, underlying the transitional character of this station.

721 At all the stations grouped into cluster 3, the calcareous species *Nonionellina labradorica*
722 was the major species with variable relative abundances. This is a typical glacier-distal
723 species, of which the distribution was often related to nutrient enrichment or to the presence
724 of AW (Hald and Korsun, 1997; Korsun and Hald, 1998). This species preferentially feeds on
725 diatoms (e.g., Cedhagen, 1991; Jernas et al., 2018) and its location at the sediment surface
726 may indicate the presence of fresh phytodetritus inputs, which is mostly composed of diatoms
727 in the inner Kongsfjorden (Lalande et al., 2016). The presence of *N. labradorica* is compatible
728 with the slightly higher organic carbon content measured in the stations of cluster 3 (0.4-0.7 %
729 of TOC) (Table 3). Indeed, the fjord dynamics, with the deep AW intrusion, consequent
730 subglacial-induced upwelling at the glacier terminus and downfjord surface advection, can
731 supply nutrients (i.e., nitrate and phosphate) in this medial area enhancing primary productivity
732 (Halbach et al., 2019). Several other minor species (e.g. *Quinqueloculina seminula*, *Labrospira*
733 *crassimargo*, *Astrononion gallowayi*, *Siphonaperta agglutinata* and *Adercotryma glomeratum*)
734 often found in Svalbard fjords (e.g., Hald and Korsun, 1997; Korsun and Hald, 2000; Forwick
735 et al., 2010; Jernas et al., 2018; Kniazeva and Korsun, 2019) were identified in the medial
736 stations and are the reason for the increased diversity measured in this area compared to the
737 innermost part of the fjord (Table 3). The fine fraction at these stations was characterised by
738 the elongated calcareous species *Stainforthia feylingi*. This species was previously found in
739 the outer Kongsfjorden (Jernas et al, 2018), but little is known about its ecology. This species
740 is reported as opportunist (e.g., Lloyd et al., 2007) and often associated to high primary
741 productivity in the vicinity of sea ice in paleoenvironmental reconstructions (e.g., Seidenkrantz,
742 2013). In August 2018, *S. feylingi* co-occurred with a phytodetritus indicator (i.e., *N.*
743 *labradorica*), which supports the speculation of its preferences for that food resource. The
744 small fraction at station St5 was dominated by the small-sized species *Pullenia* cf. *osloensis*
745 which presented high relative abundances also in the distal stations.
746 The microhabitat distribution in the >150 μm fraction showed decreased foraminiferal
747 abundances with sediment depth. The downcore microhabitat distribution of *N. labradorica*
748 showed subsurface peaks that demonstrate its capacity to occupy infaunal habitats. This

suggests a potential ability to exploit other food resources than fresh phytodetritus (e.g., buried organic matter; Corliss, 1991; Alve, 2010) or to benefit from an alternative metabolism (e.g. denitrification, Jauffrais et al., 2019). Indeed, some closely related species are capable of denitrification (e.g., *Nonionella* sp. T1 and *Nonionella* cf *stella*; Glock et al., 2019; Choquel et al., 2021) and thus can successfully occupy and exploit subsurface sediment resources. *Globobulimina auriculata* also displayed a subsurface increase at St4. This behaviour can be explained by its tolerance for low oxygen conditions and/or denitrification capacity as other *Globobulimina* species (e.g., Risgaard-Petersen et al., 2006; Koho et al., 2011) and thus able to occupy infaunal habitats where interspecific competition is reduced. The microhabitat distribution observed in the medial stations may also result from reduced sediment deposition, increased sediment stability, increase in organic flux, and therefore the development of diverse suitable ecological niches to occupy.

III. Distal biozone

The outer part of the transect was characterised by a fresh surface layer and by an intermediate water and deep layer of AW (Fig. 1). This part of the fjord, deeper than 100 m, is directly influenced by the inflow of warm and salty AW coming from the WSC current flowing along the western coast of Svalbard. The lowest values of surface turbidity were observed in this area of the fjord (Fig. S1). The increased water transparency was the result of augmented distance from the Kronebreen front. However, we observed the same type of sediment (i.e. medium silt) than upstream. This could suggest that this area is still impacted by the sedimentation from a diluted turbid plume. At St8, which is located close to the southern coast, the coarser medium silt of the fjord sediment was observed with a secondary mode of very fine sand. This may suggest sediment inputs from continental glacier meltwaters (i.e., Midtre Lovénbreen). Unfortunately, the local sedimentation rate is unknown.

The distal stations grouped into cluster 4 (St6, St8 and St9) (Fig. 3) were positively correlated with sediment organic carbon and water depth (Fig. 5). The dominant species was the agglutinated *Adercotryma glomeratum* followed by the calcareous *N. labradorica* (Fig. 3).

Adercotryma glomeratum was suggested to be able to exploit low food quality and/or quantity (Jernas et al., 2018), whereas *N. labradorica* is supposed to feed on fresh phytodetritus or to have different metabolism (i.e., able of denitrification; see references above). The coexistence of these two species may be explained by the occupation of different ecological niches. *Adercotryma glomeratum* was also previously related to AW influence in the Kongsfjorden (Jernas et al., 2018), in other western Svalbard fjords including Isfjorden and Krossfjorden (Korsun and Hald, 1997), and in the southern fjord Storfjorden (Fossile et al., 2020). The clear dominance of this species in the distal stations and its decreasing percentage in the medial area (where represented only a minor proportion of the assemblages), suggests the decline in the AW influence upstream fjord. This is coherent with AW intrusion invading the fjord trench from the outer sea and perhaps suggests a longer persistence of AW at the distal stations. At St 9, *Cibicidoides lobatulus* is highly present and could indicate high-energy near-bed currents at this station (Murray, 2006).

The fine fraction (63-150 µm) of the distal stations and were characterised by the presence of the small-sized species *Pullenia* cf. *osloensis*. The ecological preferences of *P.* cf. *osloensis* have not been previously described. *Pullenia* spp. were previously reported as detritivore and typically found on the shelf-bathyal area of cold environments (Murray, 2006). Some species of this genus are often used as AW indicators in paleoenvironmental studies (e.g., Chauhan et al., 2016 and reference therein), potentially explaining the presence of this species mostly at St5 and in the distal stations that are under the inflow of AW (Fig. S3). Moreover, *Stainforthia feylingi* showed important relative abundances at the outermost station St9 suggesting increased phytodetritus inputs at this location (e.g., Lloyd et al., 2007; Seidenkrantz, 2013).

Even if foraminiferal species composition was similar among the distal stations, the microhabitat distribution displayed some differences (Fig. 5). The subsurface peaks observed at St9 (Fig. 5) was determined by the high densities of *A. glomeratum* and *N. labradorica*. Both species may have preferred the infaunal habitat to exploit additional food resources (i.e., buried organic matter of lower quality) or use different metabolisms (i.e., denitrification) and thus reduce competition with the many species present at the sediment surface. However, *A.*

glomeratum was also present with high numbers at the sediment surface and presented a deep increase in densities at St6, that may point out to bioturbation processes at these stations (e.g., Thibault De Chanvalon et al., 2015).

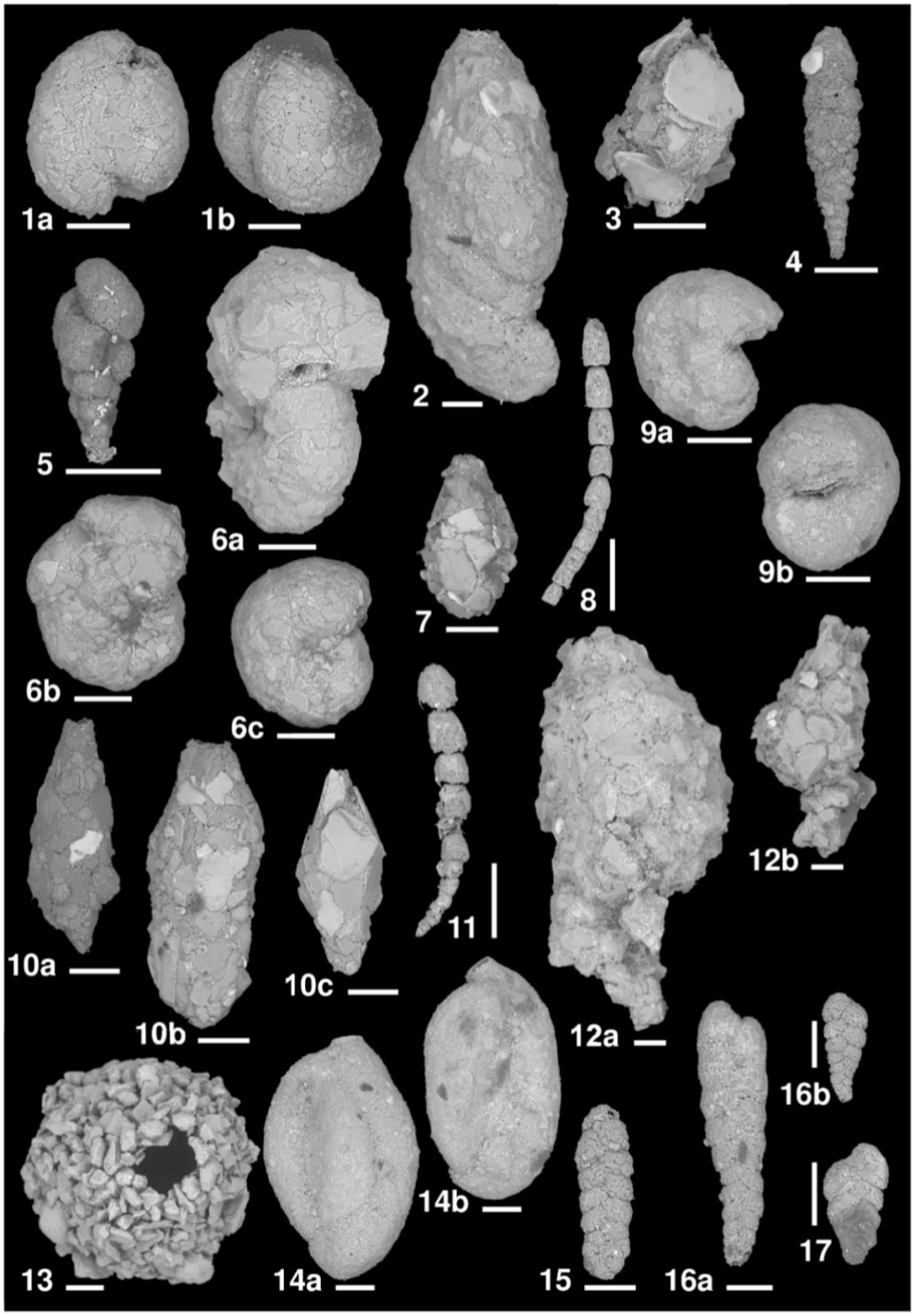

Plate 1. Scanning electron micrographs (SEM) of the most relevant agglutinated benthic species from Kongsfjorden (scale bars = 100 µm). **1a,1b.** *Adercotryma glomeratum* (Brady, 1878). **2.** *Ammotium cassis* (Parker, 1870). **3.** *Capsammina bowmanni* (Heron-Allen & Earland, 1912). **4.** *Cuneata arctica* (Brady, 1881). **5.** *Eggerella advena* (Cushman, 1922). **6a, 6b, 6c.** *Labrospira crassimargo* (Norman, 1892). **7.** *Lagenammina difflugiformis* (Brady, 1879). **8.** *Leptohalysis scottii* (Chaster, 1892). **9a, 9b.** *Recurvoides turbinatus* (Brady, 1881). **10a, 10b, 10c.** *Reophax fusiformis* (Williamson, 1858). **11.** *Reophax catella* Höglund, 1947. **12a, 12b.** *Reophax scorpiurus* Montfort, 1808. **13.** *Saccammina* cf. *sphaerica* Brady, 1871. **14a, 14b.** *Siphonaperta agglutinata* (Cushman, 1917). **15.** *Spiroplectammina biformis* (Parker & Jones, 1865). **16a, 16b.** *Textularia earlandi Parker, 1952.* **17.** *Textularia torquata* Parker, 1952.

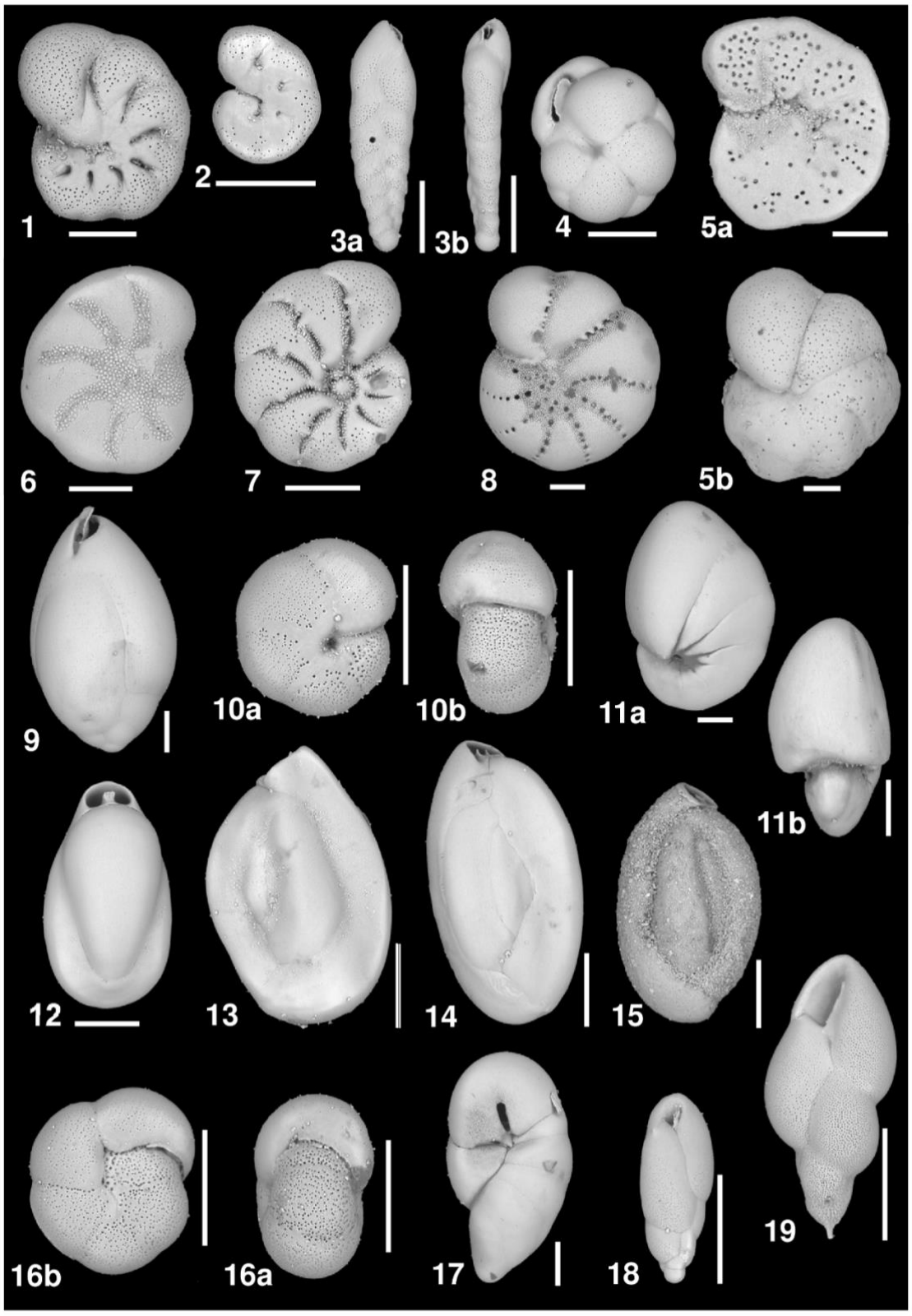

819

820 **Plate 2.** Scanning electron micrographs (SEM) of the most relevant calcareous benthic species from
821 Kongsfjorden (scale bars = 100 µm). **1a,1b.** *Astrononion gallowayi* Loeblich & Tappan, 1953. **2.**
822 *Astrononion* sp. Cushman & Edwards, 1937**. 3.** *Bolivina pseudopunctata* Höglund, 1947. **4.** *Cassidulina*
823 *reniforme* Nørvang, 1945. **5a, 5b.** *Cibicidoides lobatulus* (Walker & Jacob, 1798). **6.** *Cribroelphidium*
824 *subarcticum* (Cushman, 1944). **7.** *Elphidium clavatum* Cushman, 1930. **8.** *Elphidium bartletti* Cushman,

1933. **9.** *Globobulimina auriculata* (Bailey, 1894). **10a, 10b.** *Melonis pompilioides* (Fichtel & Moll, 1798). **11a, 11b.** *Nonionellina labradorica* (Dawson, 1860). **12.** *Pyrgo williamsoni* (Silvestri, 1923). **13.** *Quinqueloculina arctica* Cushman, 1933. **14.** *Quinqueloculina seminula* (Linnaeus, 1758). **15.** *Quinqueloculina stalkeri* Loeblich & Tappan, 1953. **16a, 16b.** *Pullenia* cf. *osloensis* Feyling-Hanssen, 1954. **17.** *Robertina arctica* d'Orbigny, 1846. **18.** *Stainforthia feylingi* Knudsen & Seidenkrantz, 1994. **19.** *Stainforthia loeblichi* (Feyling-Hanssen, 1954).

6. Conclusions

Living benthic foraminiferal faunas from the inner Kongsfjorden were studied to determine the combined influence of glacier melting with AW inflow on the benthic system. To that aim, foraminiferal patterns were investigated in relation to water masses properties, sediment characteristics and organic matter inputs to the seafloor during late summer, when environmental gradients are the steepest. Benthic environmental conditions were connected to tidewater glacier dynamics and interpreted based on the glacial-related disturbances. The surface water turbidity, water depth and the organic inputs to the seafloor are the main driving factors for foraminiferal patterns in the inner Kongsfjorden, determining the establishment of three different biozones (i.e., proximal, medial and distal) summarised in the conceptual model (Fig. 8). High surface water turbidity related to freshwater and sediment inputs from subglacial discharges and surface runoff, and reduced organic flux due to reduced primary production, were the limiting factors for the proximal biozone. This inner area was dominated by few stress-tolerant and/or opportunistic glacier proximal species restricted to the sediment surface (e.g., *Capsammina bowmanni*, *Cassidulina reniforme* and *Textularia earlandi*). A progressive reduction of the general stressful environmental conditions (i.e., reduced physical disturbance and increase organic flux) and the increased AW inflow influence in the medial and distal biozones favoured the establishment of diversified foraminiferal communities able to occupy different ecological niches and microhabitats (i.e., epifaunal and/or infaunal). In particular, the phytodetritus indicator *Nonionellina labradorica* and the AW indicator *Adercotryma glomeratum* were the representative species in the medial and distal biozone, respectively. The comparison between the two size fractions highlighted the presence of different

foraminiferal assemblages in terms of species composition but similar foraminiferal patterns along the transect. The supplementary ecological information obtained from the small size assemblage was imprecise due the lack of knowledge regarding the ecological preferences for these species in modern environments. Ultimately, the variation of several environmental parameters in relation to the distance from the glacier terminus, parallelly to the appearance of different foraminiferal assemblages, suggests the potential investigation of diversity patterns in relation to the distance from the front as potential proxy for glacier retreat.

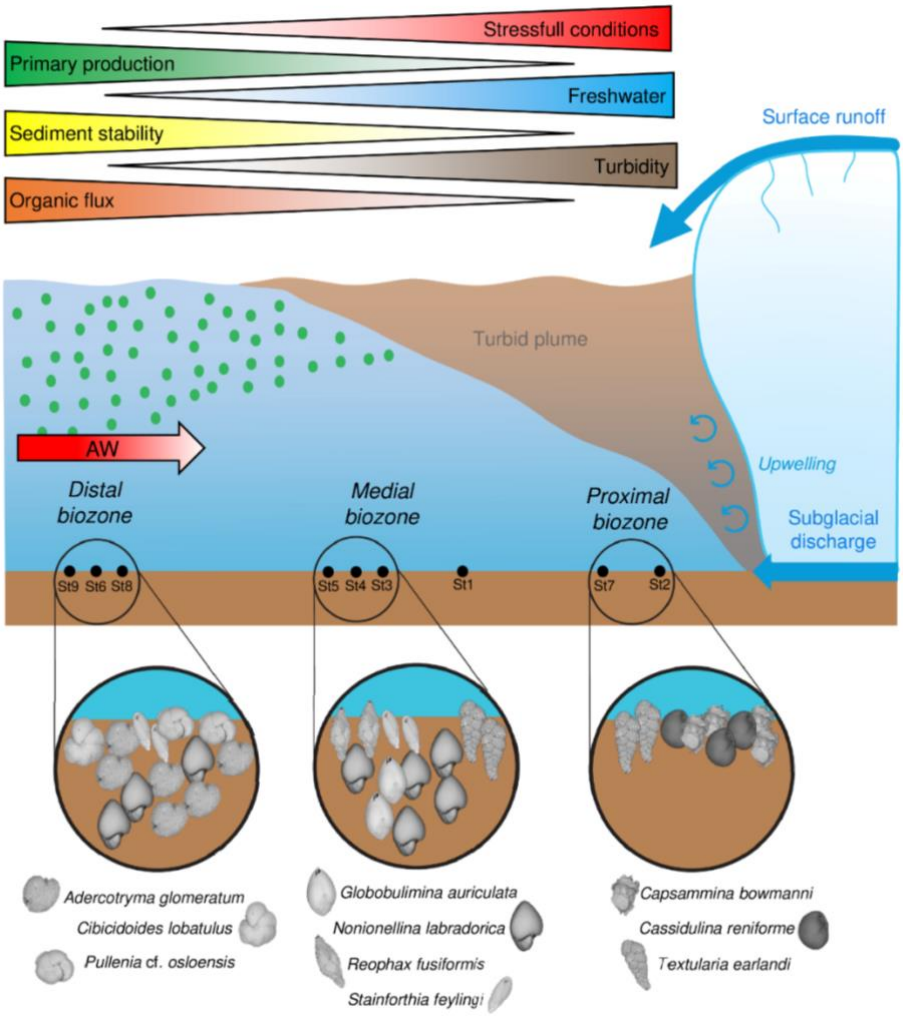

Figure 8. Conceptual model showing the environmental gradients created by tidewater glacier dynamics and, repartition of benthic foraminiferal communities and their microhabitat preferences.

Supplementary materials

Tables S1 and S2 and Figs. S1, S2, and S3 can be found in the Supplementary material. Scanning electron micrographs (plates) of the most relevant species are shown in Figs. S4, S5 and S6 in the Supplementary material.

Author contributions

EF: conceptualisation, data curation, formal analysis, investigation, methodology, validation, visualisation, writing-original draft, writing-review & editing. MM, MPN and HH: conceptualisation, funding acquisition, investigation, resources, supervision, validation, writing-review & editing. AB: funding acquisition, resources, writing-review & editing. YP: investigation, writing-review & editing. IB: methodology, writing-review & editing. MD: methodology, writing-review & editing.

Competing interests

The authors declare that they have no conflict of interest.

Acknowledgements

We thank Alain Jadas-Hecart and Nadage Blon for technical support during sediment organic matter analysis, Francois Guillory for technical support during sediment grain size analysis, Sabine Schmidt for sedimentological investigation and Katrine Husum for taxonomical support. This project benefits from the technical support of the AWIPEV French - German Arctic Research Base at Ny-Ålesund.

882 **Funding**

883 This research is part of the PhD thesis of Eleonora Fossile, which is co-funded by French
884 National Program MOPGA (Make Our Planet Great Again) and the University of Angers. The
885 field campaign was organised into the frame of IPEV logistic project C3 (Coasts under Climate
886 Change3 suite) with the collaboration of the sailing boat Aztec Lady. Sediment sampling was
887 founded by BiSMART project (University of Angers). Water column properties were measured
888 by CTD profiling in the context of the ISMOGLAC project (*ISotopic and physicalchemical*
889 *MOnitoring of GLACial drainages and sea water in the Ny-Ålesund area (Svalbard)*).

References

Alboukadel Kassambara and Fabian Mundt, 2020. factoextra: Extract and Visualize the Results of Multivariate Data Analyses. R package version 1.0.7. https://CRAN.R-project.org/package=factoextra

Alve, E., 2010. Benthic foraminiferal responses to absence of fresh phytodetritus: A two-year experiment. Mar. Micropaleontol. 76, 67–75. https://doi.org/10.1016/j.marmicro.2010.05.003

Alve, E., Korsun, S., Schönfeld, J., Dijkstra, N., Golikova, E., Hess, S., Husum, K., Panieri, G., 2016. Foram-AMBI: A sensitivity index based on benthic foraminiferal faunas from North-East Atlantic and Arctic fjords, continental shelves and slopes. Mar. Micropaleontol. 122, 1–12. https://doi.org/10.1016/j.marmicro.2015.11.001

Alve, E., Nagy, J., 1986. Estuarine foraminiferal distribution in Sandebukta, a branch of the Oslo Fjord (Norway). J. Foraminifer. Res. 16, 261–284. https://doi.org/10.2113/gsjfr.16.4.261

Arndt, S., Jørgensen, B.B., LaRowe, D.E., Middelburg, J.J., Pancost, R.D., Regnier, P., 2013. Quantifying the degradation of organic matter in marine sediments: A review and synthesis. Earth-Science Rev. 123, 53–86. https://doi.org/10.1016/j.earscirev.2013.02.008

Basedow, S.L., Eiane, K., Tverberg, V., Spindler, M., 2004. Advection of zooplankton in an Arctic fjord (Kongsfjorden, Svalbard). Estuar. Coast. Shelf Sci. 60, 113–124. https://doi.org/10.1016/j.ecss.2003.12.004

Bisutti, I., Hilke, I., Raessler, M., 2004. Determination of total organic carbon - An overview of current methods. TrAC - Trends Anal. Chem. 23, 716–726. https://doi.org/10.1016/j.trac.2004.09.003

Blott, S.J., Pye, K., 2001. GRADISTAT: a grain size distribution and statistics package for the analysis of unconsolidated sediments. Earth Surf. Process. Landforms 26, 1237–1248. https://doi.org/10.1002/esp.261

Bourgeois, S., Kerhervé, P., Calleja, M.L., Many, G., Morata, N., 2016. Glacier inputs influence organic matter composition and prokaryotic distribution in a high Arctic fjord (Kongsfjorden, Svalbard). J. Mar. Syst. 164, 112–127. https://doi.org/10.1016/j.jmarsys.2016.08.009

Bourriquen, M., Baltzer, A., Mercier, D., Fournier, J., Pérez, L., Haquin, S., Bernard, E., Jensen, M., 2016. Coastal evolution and sedimentary mobility of Brøgger Peninsula, northwest Spitsbergen. Polar Biol. 39, 1689–1698. https://doi.org/10.1007/s00300-016-1930-1

Bourriquen, M., Mercier, D., Baltzer, A., Fournier, J., Costa, S., Roussel, E., 2018. Paraglacial coasts responses to glacier retreat and associated shifts in river floodplains over decadal timescales (1966–2016), Kongsfjorden, Svalbard. L. Degrad. Dev. 29, 4173–4185. https://doi.org/10.1002/ldr.3149

Calleja, M.L., Kerhervé, P., Bourgeois, S., Kędra, M., Leynaert, A., Devred, E., Babin, M., Morata, N., 2017. Effects of increase glacier discharge on phytoplankton bloom dynamics and pelagic geochemistry in a high Arctic fjord. Prog. Oceanogr. 159, 195–210. https://doi.org/10.1016/j.pocean.2017.07.005

Caulle, C., Koho, K.A., Mojtahid, M., Reichart, G.J., Jorissen, F.J., 2014. Live (Rose Bengal stained) foraminiferal faunas from the northern Arabian Sea: Faunal succession within and below the OMZ. Biogeosciences 11, 1155–1175. https://doi.org/10.5194/bg-11-1155-2014

Cedhagen, T., 1991. Retention of chloroplasts and bathymetric distribution in the sublittoral foraminiferan *Nonionellina labradorica*. Ophelia 33, 17–30. https://doi.org/10.1080/00785326.1991.10429739

Chauhan, T., Rasmussen, T.L., Noormets, R., 2016. Palaeoceanography of the Barents Sea continental margin, north of Nordaustlandet, Svalbard, during the last 74 ka. Boreas 45, 76–99. https://doi.org/10.1111/bor.12135

Choquel, C., Geslin, E., Metzger, E., Filipsson, H.L., Risgaard-Petersen, N., Launeau, P., Giraud, M., Jauffrais, T., Jesus, B., Mouret, A., 2021. Denitrification by benthic foraminifera and their contribution to N-loss from a fjord environment. Biogeosciences 18, 327–341. https://doi.org/10.5194/bg-18-327-2021

Corliss, B.H., 1991. Morphology and microhabitat preferences of benthic foraminifera from the northwest Atlantic Ocean. Mar. Micropaleontol. 17, 195–236. https://doi.org/10.1016/0377-8398(91)90014-W

Cottier, F., Tverberg, V., Inall, M., Svendsen, H., Nilsen, F., Griffiths, C., 2005. Water mass modification in an Arctic fjord through cross-shelf exchange: The seasonal hydrography of Kongsfjorden, Svalbard. J. Geophys. Res. Ocean. 110, 1–18. https://doi.org/10.1029/2004JC002757

Cottier, F.R., Nilsen, F., Enall, M.E., Gerland, S., Tverberg, V., Svendsen, H., 2007. Wintertime warming of an Arctic shelf in response to large-scale atmospheric circulation. Geophys. Res. Lett. 34, 1–5. https://doi.org/10.1029/2007GL029948

Cottier, F.R., Nilsen, F., Skogseth, R., Tverberg, V., Skarðhamar, J., Svendsen, H., 2010. Arctic fjords: a review of the oceanographic environment and dominant physical processes. Geol. Soc. London, Spec. Publ. 344, 35–50. https://doi.org/10.1144/sp344.4

Cowton, T., Slater, D., Sole, A., Goldberg, D., Nienow, P., 2015. Modeling the impact of glacial runoff on fjord circulation and submarine melt rate using a new subgrid-scale parameterization for glacial plumes. J. Geophys. Res. Ocean. 796–812. https://doi.org/10.1002/2014JC010324

D'Angelo, A., Giglio, F., Miserocchi, S., Sanchez-Vidal, A., Aliani, S., Tesi, T., Viola, A., Mazzola, M., Langone, L., 2018. Multi-year particle fluxes in Kongsfjorden, Svalbard. Biogeosciences 15, 5343–5363. https://doi.org/10.5194/bg-15-5343-2018

Dai, A., Luo, D., Song, M., Liu, J., 2019. Arctic amplification is caused by sea-ice loss under increasing CO2. Nat. Commun. 10, 1–13. https://doi.org/10.1038/s41467-018-07954-9

David T, D., K.P., K., 2017. Recent variability in the Atlantic water intrusion and water masses in Kongsfjorden, an Arctic fjord. Polar Sci. 11, 30–41. https://doi.org/10.1016/j.polar.2016.11.004

Dickson, B., Meincke, J., and Rhines, P. (2008). "Arctic–subarctic ocean fluxes: defining the role of the northern seas in climate," in Arctic–Subarctic Ocean Fluxes, eds R. R. Dickson, J. Meincke, and P. Rhines (Dordrecht: Springer), 1–13. https://doi.org/10.1007/978-1-4020-6774-7_1

Duchemin, G., Fontanier, C., Jorissen, F.J., Barras, C., Griveaud, C., 2007. Living small-sized (63–150 µm) foraminifera from mid-shelf to mid-slope environments in the Bay of Biscay. J. Foraminifer. Res. 37, 12–32. https://doi.org/10.2113/gsjfr.37.1.12

Duros, P., Fontanier, C., Metzger, E., Cesbron, F., Deflandre, B., Schmidt, S., Buscail, R., Zaragosi, S., Kerhervé, P., Rigaud, S., Delgard, M.L., Jorissen, F.J., 2013. Live (stained) benthic foraminifera from the Cap-Ferret Canyon (Bay of Biscay, NE Atlantic): A comparison between the canyon axis and the surrounding areas. Deep. Res. Part I Oceanogr. Res. Pap. 74, 98–114. https://doi.org/10.1016/j.dsr.2013.01.004

Forwick, M., Vorren, T.O., Hald, M., Korsun, S., Roh, Y., Vogt, C., Yoo, K.-C., 2010. Spatial and temporal influence of glaciers and rivers on the sedimentary environment in Sassenfjorden and Tempelfjorden, Spitsbergen. Geol. Soc. London, Spec. Publ. 344, 163–193. https://doi.org/10.1144/SP344.13

Fossile, E., Nardelli, M.P., Jouini, A., Lansard, B., Pusceddu, A., Moccia, D., Michel, E., Péron, O., Howa, H., Mojtahid, M., 2020. Benthic foraminifera as tracers of brine production in the Storfjorden "sea ice factory." Biogeosciences 17, 1933–1953. https://doi.org/10.5194/bg-17-1933-2020

Glock, N., Roy, A.S., Romero, D., Wein, T., Weissenbach, J., Revsbech, N.P., Høgslund, S., Clemens, D., Sommer, S., Dagan, T., 2019. Metabolic preference of nitrate over oxygen as an electron

acceptor in foraminifera from the Peruvian oxygen minimum zone. PNAS 116, 2860–2865. https://doi.org/10.1073/pnas.1813887116

Gooday, A.J., Aranda da Silva, A., Koho, K.A., Lecroq, B., Pearce, R.B., 2010. The “mica sandwich”; a remarkable new genus of Foraminifera (Protista , Rhizaria) from the Nazaré Canyon (Portuguese margin , NE Atlantic) 56, 345–357. http://www.jstor.org/stable/40959488

Gooday, A.J., Goineau, A., 2019. The contribution of fine sieve fractions (63-150 µm) to foraminiferal abundance and diversity in an area of the eastern Pacific Ocean licensed for polymetallic nodule exploration. Front. Mar. Sci. 6, 1–17. https://doi.org/10.3389/fmars.2019.00114

Google Earth Pro V 7.3.3.7786 (July 26, 2016). Spitsbergen, Norway. 78°52'39.19"N, 12°35'42.51"E. Eye alt. 20 km. Maxar Technologies 2021. https://www.google.com/earth/index.html [January 25, 2021]

Graversen, R.G., Mauritsen, T., Tjernström, M., Källén, E., Svensson, G., 2008. Vertical structure of recent Arctic warming. Nature 451, 53–56. https://doi.org/10.1038/nature06502

Halbach, L., Vihtakari, M., Duarte, P., Everett, A., Granskog, M.A., Hop, H., Kauko, H.M., Kristiansen, S., Myhre, P.I., Pavlov, A.K., Pramanik, A., Tatarek, A., Torsvik, T., Wiktor, J., Wold, A., Wulff, A., Steen, H., Assmy, P., 2019. Tidewater Glaciers and Bedrock Characteristics Control the Phytoplankton Growth Environment in a Fjord in the Arctic. Front. Mar. Sci. 6. https://doi.org/10.3389/fmars.2019.00254

Hald, M., Korsun, S., 1997. Distribution of modern benthic foraminifera from fjords of Svalbard, European Arctic. J. Foraminifer. Res. 27, 101–122. https://doi.org/10.2113/gsjfr.27.2.101

Hegseth, E.N., Tverberg, V., 2013. Effect of Atlantic water inflow on timing of the phytoplankton spring bloom in a high Arctic fjord (Kongsfjorden, Svalbard). J. Mar. Syst. 113–114, 94–105. https://doi.org/10.1016/j.jmarsys.2013.01.003

Hijmans, R. J., 2019. geosphere: Spherical Trigonometry. R package version 1.5-10. https://CRAN.R-project.org/package=geosphere

Hodal, H., Falk-Petersen, S., Hop, H., Kristiansen, S., Reigstad, M., 2012. Spring bloom dynamics in Kongsfjorden, Svalbard: Nutrients, phytoplankton, protozoans and primary production. Polar Biol. 35, 191–203. https://doi.org/10.1007/s00300-011-1053-7

Holland, M.M., Bitz, C.M., 2003. Polar amplification of climate change in coupled models. Clim. Dyn. 21, 221–232. https://doi.org/10.1007/s00382-003-0332-6

Holmes, F.A., Kirchner, N., Kuttenkeuler, J., Krützfeldt, J., Noormets, R., 2019. Relating ocean temperatures to frontal ablation rates at Svalbard tidewater glaciers: Insights from glacier proximal datasets. Sci. Rep. 9, 1–11. https://doi.org/10.1038/s41598-019-45077-3

Hop, H., Pearson, T., Hegseth, E.N., Kovacs, K.M., Wiencke, C., Kwasniewski, S., Eiane, K., Mehlum, F., Gulliksen, B., Wlodarska-Kowalezuk, M., Lydersen, C., Weslawski, J.M., Cochrane, S., Gabrielsen, G.W., Leakey, R.J.G., Lonne, O.J., Zajaczkowski, M., Falk-Petersen, S., Kendall, M., Wangberg, S.A., Bischof, K., Voronkov, A.Y., Kovaltchouk, N.A., Wiktor, J., Poltermann, M., di Prisco, G., Papucci, C., Gerland, S., 2002. The marine ecosystem of Kongsfjorden, Svalbard. Polar Res. 21, 167–208. https://doi.org/10.3402/polar.v21i1.6480

Hop, H., Wiencke, C., 2019. The Ecosystem of Kongsfjorden, Svalbard. Alfred Wegener Institute, Helmholtz Centre for Polar and Marine Research, Bremerhaven, Germany. https://doi.org/10.1007/978-3-319-46425-1_1

Hopwood, M.J., Carroll, D., Dunse, T., Hodson, A., Holding, J.M., Iriarte, J.L., Ribeiro, S., Achterberg, E.P., Cantoni, C., Carlson, D.F., Chierici, M., Clarke, J.S., Cozzi, S., Fransson, A., Juul-Pedersen, T., Winding, M.H.S., Meire, L., 2020. Review article: How does glacier discharge affect marine biogeochemistry and primary production in the Arctic? Cryosphere 14, 1347–1383. https://doi.org/10.5194/tc-14-1347-2020

How, P., Benn, D.I., Hulton, N.R.J., Hubbard, B., Luckman, A., Sevestre, H., Pelt, W.J.J.V., Lindbäck, K., Kohler, J., Boot, W., 2017. Rapidly changing subglacial hydrological pathways at a tidewater glacier revealed through simultaneous observations of water pressure, supraglacial lakes, meltwater plumes and surface velocities. Cryosphere 11, 2691–2710. https://doi.org/10.5194/tc-11-2691-2017

Husum, K., Howe, J.A., Baltzer, A., Forwick, M., Jensen, M., Jernas, P., Korsun, S., Miettinen, A., Mohan, R., Morigi, C., Myhre, P.I., Prins, M.A., Skirbekk, K., Sternal, B., Boos, M., Dijkstra, N., Troelstra, S., 2019. The marine sedimentary environments of Kongsfjorden, Svalbard: an archive of polar environmental change. Polar Res. 38, 1–16. https://doi.org/10.33265/polar.v38.3380

IPCC, 2019: IPCC Special Report on the Ocean and Cryosphere in a Changing Climate [H.-O. Pörtner, D.C. Roberts, V. Masson-Delmotte, P. Zhai, M. Tignor, E. Poloczanska, K. Mintenbeck, A. Alegría, M. Nicolai, A. Okem, J. Petzold, B. Rama, N.M. Weyer (eds.)]. In press.

Jauffrais, T., LeKieffre, C., Schweizer, M., Geslin, E., Metzger, E., Bernhard, J.M., Jesus, B., Filipsson, H.L., Maire, O., Meibom, A., 2019. Kleptoplastidic benthic foraminifera from aphotic habitats: insights into assimilation of inorganic C, N and S studied with sub-cellular resolution. Environ. Microbiol. 21, 125–141. https://doi.org/10.1111/1462-2920.14433

Jernas, P., Klitgaard-Kristensen, D., Husum, K., Koç, N., Tverberg, V., Loubere, P., Prins, M., Dijkstra, N., Gluchowska, M., 2018. Annual changes in Arctic fjord environment and modern benthic foraminiferal fauna: Evidence from Kongsfjorden, Svalbard. Glob. Planet. Change 163, 119–140. https://doi.org/10.1016/j.gloplacha.2017.11.013

Jernas, P., Klitgaard Kristensen, D., Husum, K., Wilson, L., Koç, N., 2013. Palaeoenvironmental changes of the last two millennia on the western and northern Svalbard shelf. Boreas 42, 236–255. https://doi.org/10.1111/j.1502-3885.2012.00293.x

Jorissen, F.J., de Stigter, H.C., Widmark, J.G. V, 1995. A conceptual model explaining benthic foraminiferal microhabitats. Mar. Micropaleontol. 26, 3–15. https://doi.org/10.1016/0377-8398(95)00047-X

Jorissen, F.J., Wittling, I., Peypouquet, J.P., Rabouille, C., Relexans, J.C., 1998. Live benthic foraminiferal faunas off Cape Blanc, NW-Africa: Community structure and microhabitats. Deep. Res. Part I Oceanogr. Res. Pap. 45, 2157–2188. https://doi.org/10.1016/S0967-0637(98)00056-9

Kedra, M., Kuliński, K., Walkusz, W., Legezyńska, J., 2012. The shallow benthic food web structure in the high Arctic does not follow seasonal changes in the surrounding environment. Estuar. Coast. Shelf Sci. 114, 183–191. https://doi.org/10.1016/j.ecss.2012.08.015

Kniazeva, O., Korsun, S., 2019. Seasonal data on Rose Bengal stained foraminifera in the head of Kongsfjorden, Svalbard. Data Br. 25, 104040. https://doi.org/10.1016/j.dib.2019.104040

Koho, K.A., Kouwenhoven, T.J., de Stigter, H.C., van der Zwaan, G.J., 2007. Benthic foraminifera in the Nazaré Canyon, Portuguese continental margin: Sedimentary environments and disturbance. Mar. Micropaleontol. 66, 27–51. https://doi.org/10.1016/j.marmicro.2007.07.005

Koho, K.A., Piña-Ochoa, E., Geslin, E., Risgaard-Petersen, N., 2011. Vertical migration, nitrate uptake and denitrification: Survival mechanisms of foraminifers (Globobulimina turgida) under low oxygen conditions. FEMS Microbiol. Ecol. 75, 273–283. https://doi.org/10.1111/j.1574-6941.2010.01010.x

Korsun, S., Hald, M., 2000. Seasonal dynamics of Benthic Foraminifera in a Glacially Fed Fjord of Svalbard, European Arctic. J. Foraminifer. Res. 30, 251–271. https://doi.org/10.2113/0300251

Korsun, S., Hald, M., 1998. Modern benthic foraminifera off Novaya Zemlya tidewater glaciers, Russian Arctic. Arct. Alp. Res. 30, 61–77. https://doi.org/10.2307/1551746

Lalande, C., Moriceau, B., Leynaert, A., Morata, N., 2016. Spatial and temporal variability in export fluxes of biogenic matter in Kongsfjorden. Polar Biol. 39, 1725–1738. https://doi.org/10.1007/s00300-016-1903-4

Laufer-Meiser, K., Michaud, A.B., Maisch, M., Byrne, J.M., Kappler, A., Patterson, M.O., Røy, H., Jørgensen, B.B., 2021. Potentially bioavailable iron produced through benthic cycling in glaciated Arctic fjords of Svalbard. Nat. Commun. 12, 1–13. https://doi.org/10.1038/s41467-021-21558-w

Lea, J.M., Mair, D.W.F., Rea, B.R., 2014. Instruments and Methods: Evaluation of existing and new methods of tracking glacier terminus change. J. Glaciol. 60, 323–332. https://doi.org/10.3189/2014JoG13J061

Lind, S., Ingvaldsen, R.B., Furevik, T., 2018. Arctic warming hotspot in the northern Barents Sea linked to declining sea-ice import. Nat. Clim. Chang. 8, 634–639. https://doi.org/10.1038/s41558-018-0205-y

Lloyd, J., Kuijpers, A., Long, A., Moros, M., Park, L.A., 2007. Foraminiferal reconstruction of mid- to late-Holocene ocean circulation and climate variability in Disko Bugt, West Greenland. The Holocene 8, 1079–1091. https://doi.org/10.1177/0959683607082548

Lloyd, J.M., 2006. Modern Distribution of Benthic Foraminifera From Disko Bugt, West Greenland. J. Foraminifer. Res. 36, 315–331. https://doi.org/10.2113/gsjfr.36.4.315

Luckman, A., Benn, D.I., Cottier, F., Bevan, S., Nilsen, F., Inall, M., 2015. Calving rates at tidewater glaciers vary strongly with ocean temperature. Nat. Commun. 6. https://doi.org/10.1038/ncomms9566

Lydersen, C., Assmy, P., Falk-Petersen, S., Kohler, J., Kovacs, K.M., Reigstad, M., Steen, H., Strøm, H., Sundfjord, A., Varpe, Ø., Walczowski, W., Weslawski, J.M., Zajaczkowski, M., 2014. The importance of tidewater glaciers for marine mammals and seabirds in Svalbard, Norway. J. Mar. Syst. 129, 452–471. https://doi.org/10.1016/j.jmarsys.2013.09.006

Meire, L., Mortensen, J., Meire, P., Juul-Pedersen, T., Sejr, M.K., Rysgaard, S., Nygaard, R., Huybrechts, P., Meysman, F.J.R., 2017. Marine-terminating glaciers sustain high productivity in Greenland fjords. Glob. Chang. Biol. 23, 5344–5357. https://doi.org/10.1111/gcb.13801

Meredith, M., M. Sommerkorn, S. Cassotta, C. Derksen, A. Ekaykin, A. Hollowed, G. Kofinas, A. Mackintosh, J. Melbourne-Thomas, M.M.C. Muelbert, G. Ottersen, H. Pritchard, and E.A.G. Schuur, 2019: Polar Regions. In: IPCC Special Report on the Ocean and Cryosphere in a Changing Climate [H.-O. Pörtner, D.C. Roberts, V. Masson-Delmotte, P. Zhai, M. Tignor, E. Poloczanska, K. Mintenbeck, A. Alegría, M. Nicolai, A. Okem, J. Petzold, B. Rama, N.M. Weyer (eds.)]. In press.

Meslard, F., Bourrin, F., Many, G., Kerhervé, P., 2018. Suspended particle dynamics and fluxes in an Arctic fjord (Kongsfjorden, Svalbard). Estuar. Coast. Shelf Sci. 204, 212–224. https://doi.org/10.1016/j.ecss.2018.02.020

Murray, J.W., 2006. Ecology and Application of Benthic Foraminifera. Cambridge University Press, Cambridge, New York. https://doi.org/10.1017/CBO9780511535529

Norwegian Polar Institute (2021). Annual maximum temperature in the West Spitsbergen Current. Environmental monitoring of Svalbard and Jan Mayen (MOSJ). http://www.mosj.no/en/climate/ocean/temperature-salinity-fram-strait.html

Oksanen J., F. Guillaume Blanchet, Michael Friendly, Roeland Kindt, Pierre Legendre, Dan McGlinn, Peter R. Minchin, R. B. O'Hara, Gavin L. Simpson, Peter Solymos, M. Henry H. Stevens,Eduard Szoecs and Helene Wagner (2019). vegan: Community Ecology Package. R package version 2.5-6. https://CRAN.R-project.org/package=vegan

Pasculli, L., Piermattei, V., Madonia, A., Bruzzone, G., Caccia, M., Ferretti, R., Odetti, A., Marcelli, M., 2020. New cost-effective technologies applied to the study of the glacier melting influence on

physical and biological processes in Kongsfjorden area (Svalbard). J. Mar. Sci. Eng. 8. https://doi.org/10.3390/JMSE8080593

Pavlova O., Gerland S., Hop H. (2019) Changes in Sea-Ice Extent and Thickness in Kongsfjorden, Svalbard (2003–2016). In: Hop H., Wiencke C. (eds) The Ecosystem of Kongsfjorden, Svalbard. Advances in Polar Ecology, vol 2. Springer, Cham. https://doi.org/10.1007/978-3-319-46425-1_4

Pawłowska, J., Łącka, M., Kucharska, M., Szymańska, N., Koziorowska, K., Kuliński, K., Zajączkowski, M., 2017. Benthic foraminifera contribution to fjord modern carbon pools: A seasonal study in Adventfjorden, Spitsbergen. Geobiology 15, 704–714. https://doi.org/10.1111/gbi.12242

Payne, C.M., Roesler, C.S., 2019. Characterizing the influence of Atlantic water intrusion on water mass formation and phytoplankton distribution in Kongsfjorden, Svalbard. Cont. Shelf Res. 191, 104005. https://doi.org/10.1016/j.csr.2019.104005

Piquet, A.M.T., Van De Poll, W.H., Visser, R.J.W., Wiencke, C., Bolhuis, H., Buma, A.G.J., 2014. Springtime phytoplankton dynamics in Arctic Krossfjorden and Kongsfjorden (Spitsbergen) as a function of glacier proximity. Biogeosciences 11, 2263–2279. https://doi.org/10.5194/bg-11-2263-2014

Polyakov, I. V., Pnyushkov, A. V., Alkire, M.B., Ashik, I.M., Baumann, T.M., Carmack, E.C., Goszczko, I., Guthrie, J., Ivanov, V. V., Kanzow, T., Krishfield, R., Kwok, R., Sundfjord, A., Morison, J., Rember, R., Yulin, A., 2017. Greater role for Atlantic inflows on sea-ice loss in the Eurasian Basin of the Arctic Ocean. Science (80-.). 356, 285–291. https://doi.org/10.1126/science.aai8204

Pramanik, A., Van Pelt, W., Kohler, J., Schuler, T. V., 2018. Simulating climatic mass balance, seasonal snow development and associated freshwater runoff in the Kongsfjord basin, Svalbard (1980-2016). J. Glaciol. 64, 943–956. https://doi.org/10.1017/jog.2018.80

R Core Team. R, 2020. A language and environment for statistical computing. R Foundation for Statistical Computing, Vienna, Austria. https://www.R-project.org/

Risgaard-Petersen, N., Langezaal, A.M., Ingvardsen, S., Schmid, M.C., Jetten, M.S.M., Op Den Camp, H.J.M., Derksen, J.W.M., Piña-Ochoa, E., Eriksson, S.P., Nielsen, L.P., Revsbech, N.P., Cedhagen, T., Van Der Zwaan, G.J., 2006. Evidence for complete denitrification in a benthic foraminifer. Nature 443, 93–96. https://doi.org/10.1038/nature05070

Saloranta, T.M., Svendsen, H., 2001. Across the Arctic front west of Spitsbergen: High-resolution CTD sections from 1998-2000. Polar Res. 20, 177–184. https://doi.org/10.3402/polar.v20i2.6515

Schauer, U., Fahrbach, E., Osterhus, S., Rohardt, G., 2004. Arctic warming through the Fram Strait: Oceanic heat transport from 3 years of measurements. J. Geophys. Res. C Ocean. 109, 1–14. https://doi.org/10.1029/2003JC001823

Schlitzer, R., 2020. Ocean Data View User's Guide Version 5.3.0, Ocean Data View. Available online at: https://odv.awi.de

Schloerke B., Di Cook, Joseph Larmarange, Francois Briatte, Moritz Marbach, Edwin Thoen, Amos Elberg and Jason Crowley, 2021. GGally: Extension to 'ggplot2'. R package version 2.1.0. https://CRAN.R-project.org/package=GGally

Schönfeld, J., Alve, E., Geslin, E., Jorissen, F., Korsun, S., Spezzaferri, S., Abramovich, S., Almogi-Labin, A., du Chatelet, E.A., Barras, C., Bergamin, L., Bicchi, E., Bouchet, V., Cearreta, A., Di Bella, L., Dijkstra, N., Disaro, S.T., Ferraro, L., Frontalini, F., Gennari, G., Golikova, E., Haynert, K., Hess, S., Husum, K., Martins, V., McGann, M., Oron, S., Romano, E., Sousa, S.M., Tsujimoto, A., 2012. The FOBIMO (FOraminiferal BIo-MOnitoring) initiative-Towards a standardised protocol for soft-bottom benthic foraminiferal monitoring studies. Mar. Micropaleontol. 94–95, 1–13. https://doi.org/10.1016/j.marmicro.2012.06.001

Screen, J.A., Deser, C., Simmonds, I., 2012. Local and remote controls on observed Arctic warming. Geophys. Res. Lett. 39, 1–5. https://doi.org/10.1029/2012GL051598

Screen, J.A., Simmonds, I., 2010. The central role of diminishing sea ice in recent Arctic temperature amplification. Nature 464, 1334–1337. https://doi.org/10.1038/nature09051

Seidenkrantz, M.S., 2013. Benthic foraminifera as palaeo sea-ice indicators in the subarctic realm - examples from the Labrador Sea-Baffin Bay region. Quat. Sci. Rev. 79, 135–144. https://doi.org/10.1016/j.quascirev.2013.03.014

Shepherd, A.S., Rathburn, A.E., Pérez, M.E., 2007. Living foraminiferal assemblages from the Southern California margin: A comparison of the > 150, 63-150, and > 63 μm fractions. Mar. Micropaleontol. 65, 54–77. https://doi.org/10.1016/j.marmicro.2007.06.001

Skirbekk, K., Kristensen, D.K., Rasmussen, T.L., Koç, N., Forwick, M., 2010. Holocene climate variations at the entrance to a warm Arctic fjord: evidence from Kongsfjorden trough, Svalbard. Geol. Soc. London, Spec. Publ. 344, 289–304. https://doi.org/10.1144/SP344.20

Stuecker, M.F., Bitz, C.M., Armour, K.C., Proistosescu, C., Kang, S.M., Xie, S.P., Kim, D., McGregor, S., Zhang, W., Zhao, S., Cai, W., Dong, Y., Jin, F.F., 2018. Polar amplification dominated by local forcing and feedbacks. Nat. Clim. Chang. 8, 1076–1081. https://doi.org/10.1038/s41558-018-0339-y

Sundfjord, A., Albretsen, J., Kasajima, Y., Skogseth, R., Kohler, J., Nuth, C., Skarðhamar, J., Cottier, F., Nilsen, F., Asplin, L., Gerland, S., Torsvik, T., 2017. Effects of glacier runoff and wind on surface layer dynamics and Atlantic Water exchange in Kongsfjorden, Svalbard; a model study. Estuar. Coast. Shelf Sci. 187, 260–272. https://doi.org/10.1016/j.ecss.2017.01.015

Svendsen, H., Beszczynska-Møller, A., Hagen, J.O., Lefauconnier, B., Tverberg, V., Gerland, S., Ørbæk, J.B., Bischof, K., Papucci, C., Zajaczkowski, M., Azzolini, R., Bruland, O., Wiencke, C., Winther, J.-G., Dallmann, W., 2002. The physical environment of Kongsfjorden – Krossfjorden, an Arctic fjord system in Svalbard. Polar Res. 21, 133–166. https://doi.org/10.3402/polar.v21i1.6479

Szymańska, N., Pawłowska, J., Kucharska, M., Kujawa, A., Łącka, M., Zajączkowski, M., 2017. Impact of shelf-transformed waters (STW) on foraminiferal assemblages in the outwash and glacial fjords of Adventfjorden and Hornsund, Svalbard. Oceanologia 59, 525–540. https://doi.org/10.1016/j.oceano.2017.04.006

Tedstone, A.J., Nienow, P.W., Gourmelen, N., Dehecq, A., Goldberg, D., Hanna, E., 2015. Decadal slowdown of a land-terminating sector of the Greenland Ice Sheet despite warming. Nature 526, 692–695. https://doi.org/10.1038/nature15722

Thibault De Chanvalon, A., Metzger, E., Mouret, A., Cesbron, F., Knoery, J., Rozuel, E., Launeau, P., Nardelli, M.P., Jorissen, F.J., Geslin, E., 2015. Two-dimensional distribution of living benthic foraminifera in anoxic sediment layers of an estuarine mudflat (Loire estuary, France). Biogeosciences 12, 6219–6234. https://doi.org/10.5194/bg-12-6219-2015

Torsvik, T., Albretsen, J., Sundfjord, A., Kohler, J., Sandvik, A.D., Skarðhamar, J., Lindbäck, K., Everett, A., 2019. Impact of tidewater glacier retreat on the fjord system: Modeling present and future circulation in Kongsfjorden, Svalbard. Estuar. Coast. Shelf Sci. 220, 152–165. https://doi.org/10.1016/j.ecss.2019.02.005

Trusel, L.D., Powell, R.D., Cumpston, R.M., Brigham-Grette, J., 2010. Modern glacimarine processes and potential future behaviour of Kronebreen and Kongsvegen polythermal tidewater glaciers, Kongsfjorden, Svalbard. Geol. Soc. Spec. Publ. 344, 89–102. https://doi.org/10.1144/SP344.9

Vernet, M., Ellingsen, I.H., Seuthe, L., Slagstad, D., Cape, M.R., Matrai, P.A., 2019. Influence of Phytoplankton Advection on the Productivity Along the Atlantic Water Inflow to the Arctic Ocean. Front. Mar. Sci. 6, 1–18. https://doi.org/10.3389/fmars.2019.00583

Vihtakari M., 2020. PlotSvalbard: PlotSvalbard - Plot research data from Svalbard on maps. R package

version 0.9.2. https://github.com/MikkoVihtakari/PlotSvalbard

Willis, K., Cottier, F., Kwasniewski, S., Wold, A., Falk-Petersen, S., 2006. The influence of advection on zooplankton community composition in an Arctic fjord (Kongsfjorden, Svalbard). J. Mar. Syst. 61, 39–54. https://doi.org/10.1016/j.jmarsys.2005.11.013

Wlodarska-Kowalczuk, M., Pearson, T.H., Kendall, M.A., 2005. Benthic response to chronic natural physical disturbance by glacial sedimentation in an Arctic fjord. Mar. Ecol. Prog. Ser. 303, 31–41. https://doi.org/10.3354/meps303031

Yu, L., Zhong, S., Vihma, T., Sun, B., 2021. Attribution of late summer early autumn Arctic sea ice decline in recent decades. npj Clim. Atmos. Sci. 4, 1–14. https://doi.org/10.1038/s41612-020-00157-4

Zaborska, A., Pempkowiak, J., Papucci, C., 2006. Some Sediment Characteristics and Sedimentation Rates in an Arctic Fjord (Kongsfjorden, Svalbard). Annu. Environ. Prot. 8, 79–96.

Zwally, H.J., Abdalati, W., Herring, T., Larson, K., Saba, J., Steffen, K., 2002. Surface Melt – Induced Acceleration of Greenland Ice-Sheet Flow. Science, 297, 218–222. https://doi.org/10.1126/science.1072708